Redox Biology 11 (2017) 144–156

Contents lists available at ScienceDirect

Redox Biology

journal homepage: www.elsevier.com/locate/redox

Research Paper

Deficiency in Duox2 activity alleviates ileitis in *GPx1*- and *GPx2*-knockout mice without affecting apoptosis incidence in the crypt epithelium

Fong-Fong Chu[a,b,f,*], R. Steven Esworthy[b], James H. Doroshow[c], Helmut Grasberger[d], Agnes Donko[e], Thomas L. Leto[e], Qiang Gao[a], Binghui Shen[b]

[a] Department of Gastroenterology and Hepatology, The First Affiliated Hospital and College of Clinical Medicine of Henan University of Science and Technology, Luoyang, Henan 471003, China
[b] Department of Cancer Genetics and Epigenetics, Beckman Research Institute of City of Hope, Duarte, CA 91010, USA
[c] Center for Cancer Research and Division of Cancer Treatment and Diagnosis, National Cancer Institute, Bethesda, MD 20892, USA
[d] Department of Medicine, University of Michigan, Ann Arbor, MI 48109, USA
[e] National Institute of Allergy and Infectious Diseases, Bethesda, MD 20892, USA
[f] Department of Cancer Genetics and Epigenetics, Beckman Research Institute of City of Hope, 1450 E Duarte Road, Duarte, CA 91010, USA

ARTICLE INFO

Keywords:
Glutathione peroxidase
NADPH oxidase
Dual oxidase-2
Very-early-onset inflammatory-bowel-disease
Double-knockout mouse

ABSTRACT

Mice deficient in glutathione peroxidase (GPx)-1 and -2 (*GPx1*$^{-/-}$*GPx2*$^{-/-}$ double knockout or DKO mice) develop very-early-onset (VEO) ileocolitis, suggesting that lack of defense against reactive oxygen species (ROS) renders susceptibility to intestinal inflammation. Two members of ROS-generating NADPH oxidase family, NOX1 and DUOX2, are highly inducible in the intestinal epithelium. Previously, we reported that *Nox1* deficiency ameliorated the pathology in DKO mice (*Nox1*-TKO). The role of Duox2 in ileocolitis of the DKO mice is evaluated here in *Duoxa*-TKO mice by breeding DKO mice with *Duoxa*$^{-/-}$ mice (*Duoxa*-TKO), which do not have Duox2 activity. Similar to *Nox1*-TKO mice, *Duoxa*-TKO mice no longer have growth retardation, shortened intestine, exfoliation of crypt epithelium, crypt abscesses and depletion of goblet cells manifested in DKO mice by 35 days of age. Unlike *Nox1*-TKO mice, *Duoxa*-TKO mice still have rampant crypt apoptosis, elevated proliferation, partial loss of Paneth cells and diminished crypt density. Treating DKO mice with NOX inhibitors (di-2-thienyliodonium/DTI and thioridazine/THZ) and an antioxidant (mitoquinone/MitoQ) significantly reduced gut pathology. Furthermore, in the inflamed human colon, DUOX protein expression is highly elevated in the apical, lateral and perinuclear membrane along the whole length of gland. Taken together, we conclude that exfoliation of crypt epithelium, but not crypt apoptosis, is a major contributor to inflammation. Both Nox1 and Duox2 induce exfoliation of crypt epithelium, but only Nox1 induces apoptosis. NOX1 and DUOX2 may be potential therapeutic targets for treating ileocolitis in human patients suffering inflammatory bowel disease (IBD).

1. Introduction

Elevation in reactive oxygen species (ROS) is well recognized as an essential factor in the pathogenesis of GI mucosal diseases, including peptic ulcers, inflammatory bowel disease (IBD), and GI cancers [1]. Among the well-known sources of ROS are the mitochondrial-respiratory chain and the respiratory burst produced by the NADPH oxidase-2 (NOX2) enzyme complex present in the phagocytes (e.g. neutrophils and monocytes).

Two other members of the NADPH oxidase family, NOX1 and DUOX2, are expressed in the epithelium of the lower GI tract [2,3]. The NOX1 complex produces superoxide whereas the DUOX2 complex produces H_2O_2. Their ileum and colon expression is induced from low-basal levels in response to bacterial colonization of germ-free (B6 and

Abbreviations: 129, 129S1/SvimJ; B6, C57BL6/J; DKO, double knockout of *GPx1* and *GPx2* genes; DUOX 2, dual oxidase-2; Duoxa, Duox activator; Duoxa-TKO, triple-knockout mice with disrupted *Duoxa*, *GPx1* and *GPx2* genes; DSS, dextran sodium sulfate; DTI, di-2-thienyliodonium; GFP, green fluorescent protein; GI, gastrointestinal; GPx1/2, glutathione peroxidase-1 and -2; H & E, hematoxylin and eosin; Hmox1, heme oxygenase-1; IBD, inflammatory bowel disease; IHC, immunohistochemistry; IQR, interquartile range; Lyz1, lysozyme 1; MitoQ, mitoquinone; Mmp, metalloproteinase; Non-DKO, mice having a wild-type allele of *GPx1* or *GPx2*; MPO, myeloperoxidase; NCF1, neutrophil cytosolic factor 1, aka p47phox; NOX, NADPH oxidase; NOX2, gp91phox, aka Cybb or cytochrom b-245 beta polypeptide; Nox1-TKO, triple-knockout mice with disrupted *Nox1*, *GPx1* and *GPx2* genes; nsSNP, non-synonymous single-nucleotide polymorphism; ROS, reactive oxygen species; SD, standard deviation; T4, L-thyroxine; THZ, thioridazine; TKO, triple knockout; TNFR1, tumor-necrosis-factor receptor 1; TUNEL, terminal-deoxynucleotidyl-transferase-mediated dUTP nick end labeling; VEO, very-early-onset; WT, wild-type

* Correspondence to: The First Affiliated Hospital and College of Clinical Medicine of Henan University of Science and Technology, Luoyang, Henan 471003, China.
E-mail address: fchu@coh.org (F.-F. Chu).

http://dx.doi.org/10.1016/j.redox.2016.11.001
Received 24 October 2016; Accepted 4 November 2016
Available online 22 November 2016

129 strain) mice [4,5]. *NOX1* and *DUOX2* genes are moderately and highly induced, respectively, in the ileum and colon of IBD patients compared to healthy controls [6–8]. The inflammation-associated induction of Nox1 gene expression is also exhibited in the ileum of B6- and 129-strained GPx1/2-DKO (DKO here after) [9]. Duox2 mRNA was elevated in the ileum of 129, but not B6, DKO ileum, due to WT B6 ileum having a high level of Duox2 mRNA [9]. The fact that DKO mice without Nox1 gene expression (*Nox1-GPx1/2*-TKO or *Nox1*-TKO) have ameliorated ileocolitis raises the question whether DUOX2 contributes to gut inflammation in the DKO mice. To study the impact of DUOX2 in the intestine of the DKO mice, we bred Duoxa-KO mice with DKO mice to create *Duoxa-GPx1/2*-TKO (*Duoxa*-TKO) mice. *Duoxa*-KO disabled *Duoxa1* and *Duoxa2* gene expression; the Duoxa1 and Duoxa2 are accessory proteins required for Duox1 and Duox2 enzymatic activity [10]. In the intestine, DUOX1 is barely expressed [5]. Therefore, the major impact of the Duoxa-KO is suppressing Duox2 activity in the intestine.

The histopathological features of DKO mice include elevated levels of apoptosis and anoikis (exfoliation and subsequent apoptosis) in the crypt epithelium, depletion of mature Paneth and goblet cells, as well as crypt abscesses. All of these morphological features have been associated with inflammation in other studies. The high levels of apoptosis in crypt epithelium found in the intestines of IBD patients may permit leakage of bacterial products into the circulation [11,12]. Exfoliation of intestinal epithelium is linked to increased bi-directional permeability and is associated with relapse in IBD [13]. Paneth cells are essential for limiting translocation of pathogenic bacteria across the intestinal barrier [14]. It is unclear whether any of these morphological changes is a dominating factor for inflammation.

Because some NOX inhibitors have efficacy in ameliorating ROS-associated injury, we also examined the value of monotherapy with NOX inhibitors or antioxidants in the DKO mice to test their efficacy in alleviating gut inflammation [15]. The NOX inhibitors studied were DTI (an iodonium-class flavin dehydrogenase inhibitor) [21], celastrol [18,22,23], ebselen [19], GKT137831 (a pyrazolopyridine dione analog) [24] and THZ (an N-substituted phenothiazine) [25]. The antioxidants tested were MitoQ (a mitochondria-targeted antioxidant), which had been shown to alleviate DSS-induced colitis [26], as well as caffeic acid [27] and deferoxamine mesylate [28]. The latter two compounds also have iron-chelating activity. The Nox1 inhibitors tested were selected based on their bioavailability in animals [15–20]. The best small molecule inhibitors identified will be used as scaffolds for further modification to be developed into more specific Nox1 inhibitors.

In this study, we demonstrated that Duox2 also contributes to the ileocolitis phenotype of DKO mice. However, unlike *Nox1*-TKO mice which no longer have pathology, the *Duoxa*-TKO mice still exhibit abundant apoptosis in crypt epithelium, elevated cell proliferation, partial loss of Paneth cells and decreased crypt density. Because *Duoxa*-TKO mice were healthy, we conclude that elevated levels of exfoliation in the crypt compartment, but not apoptosis in the crypt epithelium is an indicator for inflammation. In the inflamed human tissue, DUOX is also expressed in the crypt epithelium. Our drug treatment study in the DKO model suggests that targeting of Nox1 and Duox2 may be a strategy to prevent or treat ileocolitis in IBD patients.

2. Materials and methods

2.1. Mice

We bred DKO mice with *Duoxa*-KO [10] and *Nox1*-KO [29] mice all in the C57BL/6J (B6) background. The *Duoxa*-TKO line was supplemented with L-thyroxine (T4) to maintain the euthyroidism following the described procedure [10]. Some $Duoxa^{+/+}$ and $Duoxa^{+/-}$ mice were treated with vehicle by the same routes (subcutaneously from day 5 to 20, and in drinking water afterwards) to observe the T4 effect on mice. All studies were approved by the City of Hope Institutional Animal Care and Use Committee.

2.2. Disease analysis

Mouse body weight and disease signs (perianal alopecia, wet tail, and diarrhea) were monitored daily from 5 to 35 days of age before euthanasia. B6 DKO mice begin to have ileitis at 27 days of age [9]. The lengths of the small intestine and colon (ileocecal junction to anus) were recorded as an indication of inflammation. Prior analysis of mice showed that GPX2 activity is readily detectable in the ileum (the distal half of the small intestine) [30,31]. Knockout of *Gpx2* alone shows increased crypt apoptosis in the ileum and colon [32], and the ileum is the consensus site of the pathology in the small intestine of DKO mice. Within the ileum, no marked regional variation in pathology is noted in the diseased mice by 35 days of age. In the large intestine, the cecum shows pathology, while the upper colon has mild or no pathology, and the rectum has the strongest pathology [33,34]. For sample collection, 1 cm of the distal ileum (ileocecal junction) and rectum was immersed in RNAlater (Life Technologies) and processed for RNA isolation. Two adjacent 1-cm sections of the ileum and a single 1-cm section at mid-colon were frozen as backup samples. The next 4 cm of the ileum and the remaining cecum and colon were fixed in phosphate-buffered formalin for histological analysis.

Table 1
Ileum 12-Point Pathology Scoring Criteria.

Scores	0	0.5	1	1.5	2	3
Inflammation intensity[a]	0	–[b]	low	–	medium	high
Inflammation foci/field[c]	0	–	0.01–0.20	–	0.21–0.50	> 0.50
Crypt density[d]	≥39.1	–	33.6–39.0	–	27.8–33.5	22–27.7
Apoptosis/ crypt[e]	0–0.1	–	> 0.1	–	–	–
Frac. crypt w/Paneth cells[f]	0.8–1	0.6–0.79	0.34–0.59	0.15–0.33	0–0.14	–

[a] Inflammation intensity score was based on the general impression of the peak inflammatory pathology in the section. For B6 *GPx1/2*-DKO mice, this score usually is at 0–1; the score of 1 indicates isolated, small crypt abscesses. A value of 2 denotes large crypt abscesses and 3 denotes significant erosion/ulceration of the epithelium; the latter observed often in B6;129 and 129 strain *GPx1/2*-DKO mice and very rarely in B6 GPx1/2-DKO mice.

[b] Dash means no score was given for the specific parameter.

[c] The inflammation foci per field was determined by counting total number of crypt abscesses or areas of erosion per 10x field (2 mm, both sides of ileum/colon).

[d] Crypt density was rated by estimating the average number of crypts per 10x field from 4 to 6 of 10x fields (one side only).

[e] Apoptotic cells per crypt were determined by counting H & E stained cells with apoptotic figure from 100 to 200 crypts. This score was revised from our previous 0–3 scale to 0–1 to distinguish normal levels (0–0.1 per crypt) found in control mice from above normal levels (> 0.1) in the DKO mice. Down grading the apoptosis count in the pathology score was done because unlike other parameters, the apoptotic cell count was not correlated to the final pathology score (R^2=0.25) or to any other measures. The colon pathology scoring was altered from previous studies only for the apoptosis category.

[f] The fraction of Ileum crypts with visible mature Paneth cells was averaged from counting 4–6 10X fields (one side only) and based on the visible eosinophilic granules.

2.3. Histopathology scoring

A 12-point scoring system was revised from our previous 14-point system to better account for the mild histopathology in B6 ileum (Table 1) [9]. The hallmarks of DKO histopathology include high levels of crypt apoptosis and Paneth cell loss [9]. The scores from all parameters were added to assess the overall pathology; the maximum score for B6 DKO pathology was at 10 in this study. Apoptosis was scored by both histology on sections stained by hematoxylin and eosin (H & E) and TUNEL assay. The *Nox1*-TKO mice analyzed here were a new cohort of 35-day-old rather than of 50-day-old in the previous study [9]. Crypt exfoliation was counted as a non-scoring criterion; the number of crypts having at least one exfoliated epithelial cells (in the absence of neutrophils) was counted per 10X field (2 mm).

2.4. Histochemistry and immunohistochemistry (IHC)

TUNEL (ApopTag Peroxidase In Situ Apoptosis Detection Kit; Millipore) was performed on 38 samples to verify the morphological analysis of apoptotic figures. Among them, 24 were done with standard proteinase K pre-treatment, DAB for HRP substrate and hematoxylin counterstaining. Fourteen samples were done with double IHC with TUNEL first and then rabbit monoclonal anti-lysozyme 1 (Lyz1) Ab (1/1000X, ab108508, Abcam). Antigen retrieval in these 14 samples was done by microwave in citrate buffer (pH 6) without proteinase K treatment. TUNEL IHC was done with ImmPACT SG Peroxidase substrate (SK-4705, Vector Lab) to yield a blue-grey color, followed by Lyz1 IHC using an alkaline phosphatase-tagged secondary Ab and Red Alkaline Phosphatase Substrate kit (SK-5100, Vector) to yield a red color to detect Paneth cells without counterstain. Standard anti-Lyz1 IHC (DAB substrate; hematoxylin counterstain) was also used to detect Paneth cells. Anti-myeloperoxidase (MPO) antibody (PA5-32512, Thermo Scientific) IHC was performed to estimate MPO+ cells in the submucosa and to confirm crypt abscesses. Macrophages were stained with anti-CD68 (1/50X, ab31630, Abcam) and counted from 4 to 7 of 20X fields. Cells with double-stranded DNA breaks were counted by IHC+ nuclei with anti-phospho-γH2AX antibody (1/1000X, PA1-25001, pSer139, Pierce) per crypt from 17 to 43 crypts [35]. Proliferating cells were counted by anti-KI-67+ IHC (1/20X, No. M7249, DAKO Cytomation). The goblet cells were stained by Alcian blue and the sections counterstained with Nuclear Fast Red. The goblet cells were averaged from counts of 24–50 colon glands or ileum crypt.

2.5. Quantitative real-time PCR (qPCR)

RNA was isolated using a Qiagen RNeasy kit (Promega, Madison, WI). cDNA was prepared from 2 μg of total RNA following manufacturer's protocol. qPCR was performed using Taqman primers (Supplementary Table 1) using BioRad CFX96 for 40 cycles. The Ct value was determined by the ΔΔCT method normalized with β-actin. The sample numbers are shown in figure legends.

2.6. B6 and 129 Duox2 allele activity assessments

The full-length murine B6 cDNA was purchased from DNAFORM (Clone ID: 100061649; Yokohama City, Japan). The cDNA was mutated to produce four variants, one each for 3 non-synonymous SNPs detected between B6 and 129 alleles, corresponding to amino acid residues A378G, V495D and H627R. The 4th complete 129 allele variant was generated by combining all three individual SNPs. The Duox2 cDNAs in pcDNA5/FRT plasmid were transfected into mouse rectum cancer CMT93 cells, which were co-transfected with a mouse *Duoxa2* cDNA and GFP [38]. Forty-eight hours after transfection, cells were distributed in 96-well white-luminescence plates in 200 μl HBSS plus Mg^{++} and Ca^{++} and stimulated with 1 μM ionomycin or 1 μM phorbol myristate acetate to elicit activity at 37 °C. Hydrogen peroxide output was measured for 1 h at 1-min intervals by luminescence detected by 1 mM luminol and 20 μM HRP from 5×10^5 cells and the output was integrated. A GFP plasmid was co-transfected with *Duox2* cDNA to monitor overall transfection efficiency in repeated experiments and the DUOX activity level was normalized against GFP intensity. All measurements were carried out in triplicate.

2.7. Human biopsies

The colon biopsies were collected from colitis patients diagnosed at the First Affiliated Hospital of Henan University of Science and Technology. The adjacent normal appearing tissue of each patient was taken at 5 cm from the inflamed area under endoscopy. The colitis pathology was confirmed by two staff pathologists on H & E sections. IHC was performed with mouse monoclonal anti-human DUOX Ab (S-12 mAb, 250X), which does not cross react with mouse Duox [36]. Informed consent was obtained from all patients and the study was approved by the Clinical Research Ethics Committee of the Hospital.

2.8. Treating DKO mice with small molecule NOX inhibitors and antioxidants

The small molecules studied, including doses, routes and schedule of administration and mode of action are listed in Table 2. All compounds were administered orally except for di-2-thienyliodnium (DTI; Drug Synthesis & Chemistry Branch, NCI) which was also administered i.p in water in different trials and desferoxamine mysylate (Sigma). Oral drugs were administered with 1.2% methyl cellulose, 0.1% polysorbate 80 in water as the vehicle; these include DTI, caffeic acid (Sigma), celastrol (Sigma), ebselen (A.G. Scientific Inc., San Diego, CA), GKT137831 (Genkyotex, Geneva, Switzerland) and THZ (Sigma). Mitoquinone (MitoQ, Amazon) was provided in the water supply [26,37]. Three mice treated with DTI, i.p. became morbid and were euthanized immediately. Five of the 23-day-old mice were skipped for

Table 2
Small molecule drugs evaluated for treatment of ileitis in the DKO mice.

Drug name	Dose	Regiment	Biological activities
di-2-Thienyliodonium/DTI	6 mg/kg	once a day, i.p.	Inhibits flavoprotein dehydrogenases, including NOXs [21]
DTI	6 mg/kg	twice daily, gavage[a]	
Caffeic acid	60 mg/kg	once a day, gavage	Free-radical quencher, iron chelator [27]
Celastrol	1 mg/kg	once a day, gavage	Inhibits NOX1/2/4/5 and mitochondrial complex 1, induces ROS [18,22,23]
Deferoxamine mesylate	150 mg/kg	once a day, i.p.	Iron chelator [28]
Ebselen	10 mg/kg	twice daily, gavage	GPx mimetic, NOX1/2 inhibitor [19]
GKT137831	40 mg/kg	once a day, gavage	Inhibits NOX1/4 in cell-free assay [24]
Mitoquinone/ MitoQ	250 μM	in drinking water[b]	Mitochondrial antioxidant [26,37]
Thioridazine	30 mg/kg[c]	once a day, gavage	Inhibits NOXs and dopamine D2 receptors [25]

[a] Oral drug was mixed with 1.2% methyl cellulose, 0.1% polysorbate 80 in water.
[b] MitoQ was administered in drinking water (170 mg/L or 250 μM) from 22 to 35 days of age. Water was refreshed once every 3 days.
[c] Thioridazine is used as an antipsychotic and anthelmintic drug and is considered safe at 70 mg/kg and becomes lethal at 160 mg/kg in mice [20].

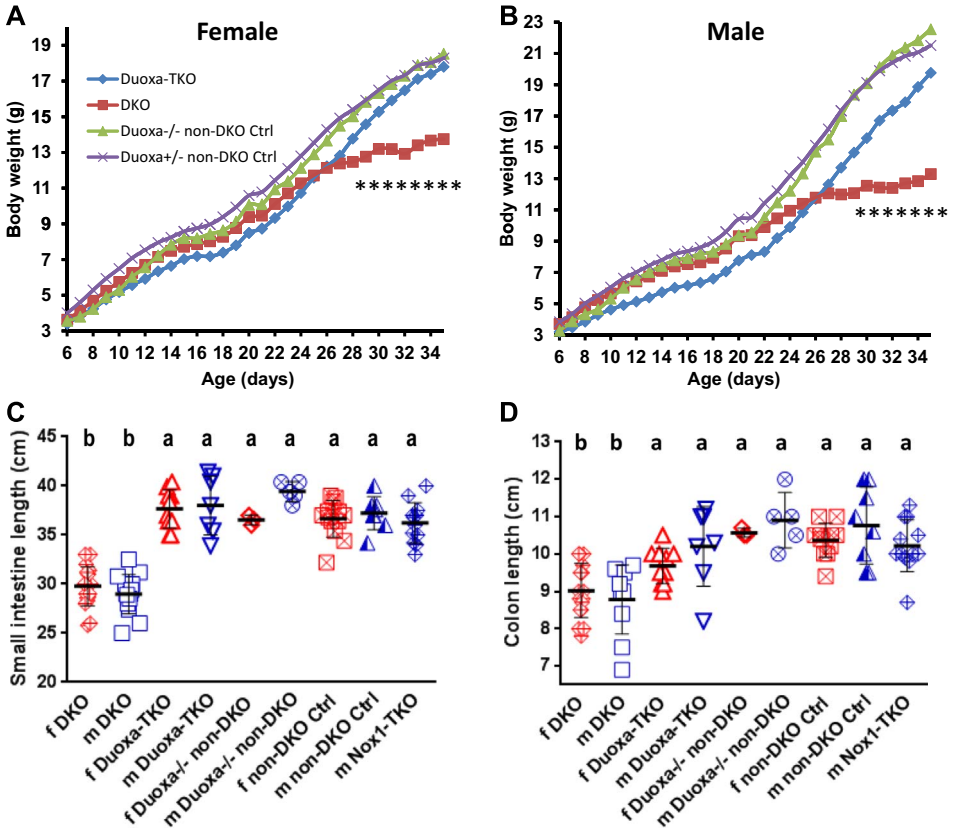

Fig. 1. Duoxa deficiency (*Duoxa*-TKO) prevents development of growth retardation and shortened small and large intestines in the DKO mice. Panels A and B are growth curves of females (f) and males (m) from 6 to 35 days of age. All mice were treated with T4. The T4-treated 35-day-old non-DKO mice ($GPx1^{+/-}GPx2^{-/-}$ or $GPx1^{-/-}GPx2^{+/-}$) weighed slightly more than non-treated non-DKO mice although not significantly. The male *Duoxa*-TKO mice were significantly smaller than DKO mice from 8 to 21 days of age due to 2 runts that thrived after weaning. The numbers of f and m mice are 11 and 8 *Duoxa*-TKO, 19 and 18 DKO, 3 and 6 $Duoxa^{-/-}$ non-DKO (Ctrl), and 13 and 7 $Duoxa^{+/-}$ non-DKO (Ctrl). There is significant difference in body weight from 28 (P=0.033) to 35 days between female DKO and *Duoxa*-TKO mice and from 29 (P=0.032) to 35 days for males; at 35 days, P=0.000015 for females and P=0.00031 for males. Panels C and D are length of small and large intestines in T4-injected sets. Bars indicate means ± SD. Analysis is done by 1-way ANOVA on DKO vs. the rest of the same gender.

the 2nd THZ dose due to slow recovery from sedation (observed in all treated mice up to 24 h) and one mouse succumbed. THZ at 70 mg/kg is considered safe, but at 160 mg/kg becomes lethal [20]. No adverse effect was observed at the subsequent administrations of THZ. Control DKO and *Nox1*-TKO mice were gavaged with vehicle or injected i.p. with PBS as reference sets. Drug treatment commenced on 22-day-old mice and was terminated at 35 days of age.

2.9. Statistical analysis

Statistical evaluation was performed using GraphPad Prism-X6. Results are shown either as mean ± standard deviation (SD) or median ± interquartile range (IQR). This choice was made based on the analysis of the parametric distribution of data (D'Agostino and Pearson omnibus normality test) or a priori knowledge of non-parametric structure (pathology scores). The corresponding statistical tests are 1-way ANOVA with Dunnett's multiple corrections for parametric data and Kruskal-Wallis with Dunn's multiple-comparison test for non-parametric data. In some cases, pair-wise *t*-tests or Mann-Whitney tests was performed to augment the analysis. The qPCR data are analyzed by pair-wise *t*-tests. The groups with different letter designations in each figure are different, where a > b > c (α=0.05). The groups sharing a same letter are not different; e.g. ab is not different from a or b group. Generally, the significance is adjusted for multiple comparisons of each set sequentially against the remaining samples, exceptions noted in the figure legends. In scatter plots, each symbol represents a single mouse.

3. Results

3.1. Improved health in the Duoxa-TKO mice

We have previously shown that disruption of the *Nox1* gene in the *Nox1*-TKO mice completely abolished the disease present in DKO mice [9]. NOX1 can form an enzyme complex in endosomes to generate ROS intracellularly in addition to extracellularly [39,40]. DUOX2 is expressed in the apical surface of un-inflamed ileum and colon also to generate ROS intracellularly and extracellularly [4,38]. We explored whether DUOX2 also contributes to DKO gut pathology. Similar to *Nox1*-TKO, the DKO mice deficient in DUOX activity by disruption of *Duoxa* genes (*Duoxa*-TKO) also have near normal weight gain especially after weaning (Fig. 1A, B). The primary impact of the *Duoxa*-KO construct in the gut is from losing DUOX2 activity since *Duox1* is not expressed there [5,41]. *Duoxa*-TKO mice also have normal lengths of ileum and colon (Fig. 1C, D).

3.2. Diminished ileal pathology in the Duoxa-TKO mice

Unlike *Nox1*-TKO mice, which have normal ileal histology, *Duoxa*-TKO mouse ileum has rampant crypt apoptosis, which is a hallmark of DKO pathology as demonstrated by apoptotic figures and TUNEL assay (Figs. 2A-C, 3A, C, 4A). Attributable to elevated crypt apoptosis, crypt density in the *Duoxa*-TKO mice is reduced (to 86%) compared to controls but still higher than in DKO mice (74% of control) (Fig. 4B). The crypt cell proliferation scores in the *Duoxa*-TKO mice are also in between the DKO and non-DKO control mice (Fig. 4C), whereas the

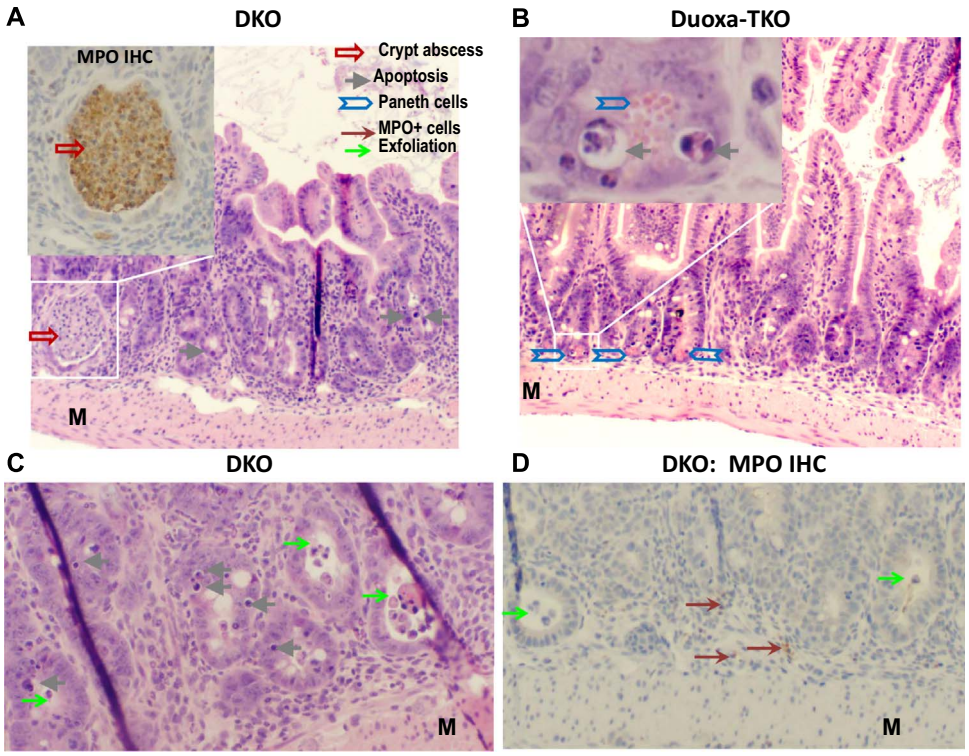

Fig. 2. Rampant apoptosis, a hallmark of DKO ileal pathology, remains prominent in *Duoxa*-TKO mice. Panel A, C and D show DKO ileum stained by H & E or MPO IHC. The insert in Panel A shows an MPO+ crypt abscess; 50% of DKO mice have crypt abscesses in minimally 1 out of 9 10X fields. The DKO ileum has crypt distortion with shortened villi. Panel B shows H & E stained, normal-length *Duoxa*-TKO ileum. The insert shows apoptotic figures in the crypt next to a Paneth cell with eosinophilic granules. Panel C shows apoptotic cells in the crypt epithelium and exfoliated cells. Panel D that shows MPO- exfoliated cells; some MPO+ cells are in the submucosa. M, muscular layer.

Nox1-TKO mice don't have elevated cell proliferation [9]. Because of the high number of apoptotic cells and partial loss of Paneth cells in the crypt, the total pathology scores of the *Duoxa*-TKO mice are intermediate between the non-DKO controls ($Gpx1^{+/-}Gpx2^{-/-}$ and $Gpx1^{+/-}Gpx2^{-/-}$) and DKO mice (Figs. 3E, 4D).

We compared the pathology scores obtained from morphological analysis on H & E stained and TUNEL IHC sections on the same mice to determine if we can rely on H & E alone to quantify pathology. Examining histopathology scores for 79 ileum samples analyzed for apoptosis by both TUNEL and H & E on DKO, *Nox1*-TKO and Duoxa-TKO mice in recent years shows that only two (*Nox1*-TKO ileum) would be altered (1 up; 1 down) (Supplementary Fig. 1). The two samples were near the threshold of 0.1 apoptotic bodies per crypt by both methods. By comparing TUNEL+ samples and MPO IHC (assessing apoptosis in the hemotoxylin stained background) (Supplementary Fig. 2), we estimated that misidentification of infiltrating lymphocytes as apoptotic bodies occurred at a level of 5–10% of the average apoptosis fraction in the DKO and *Duoxa*-TKO mice. Therefore, further pathology analysis (104 drug treated, 36 developmental study and 12 from the *Duoxa*-TKO set) was done by H & E-stained histology alone.

Duoxa-TKO ilea don't have other pathology of DKO ilea, such as inflammation foci/crypt abscesses (scored), as well as crypts with exfoliation, elevation of MPO+ cells in the submucosa and loss of goblet cells (non-scored) (Figs. 2A, D, 4E–H). However, similar to DKO ilea, *Duoxa*-TKO ilea had slightly elevated macrophage numbers compared to the non-DKO mice (Fig. 4I). The pathology observed in these mice was not contributed by T4 treatment, since vehicle-treated DKO $Duoxa^{+/-}$ or $Duoxa^{+/+}$ mice generated from the same breeders had aggregate values for each parameter indistinguishable from the T4-treated mice (data not shown).

3.3. Paneth cell loss in the DKO ileum apparently results from crypt cell apoptosis and exfoliation

Although DKO mice have lost most of their Paneth cells, it is unclear whether this loss is due to exfoliation or apoptosis, in situ. Here, we used anti-Lyz1 IHC either alone or combined with TUNEL IHC to identify exfoliated Paneth cells and apoptotic Paneth cells, in situ (Fig. 5A–C, Supplementary Fig. 3). Some Paneth cells located in the ileum crypt were positively stained with TUNEL IHC (blue-grey color) and anti-Lyz1 IHC (red-brown color), indicating that they are undergoing apoptosis in the crypt (Supplementary Fig. 3). Some Paneth cells are exfoliated into the lumen. Clearly, Paneth cell loss in the DKO ilea is via both apoptosis, in situ, and exfoliation.

Because we and others have been using H & E stained histology to identify Paneth cells by their eosinophilic granules and crypt localization, we also compared the results obtained from H & E stained sections and anti-Lyz1 IHC. IHC detection is more sensitive than morphological analysis by capturing more Paneth cells. The difference between the non-DKO control and DKO mice detected by anti-Lyz1 IHC is 9-fold vs 24-fold by histology. Likewise, the fraction of crypts with Paneth cells is 0.09 by anti-Lyz1 IHC (data not shown) vs. 0.035 by histology in the DKO mice (Fig. 4D). However, the assessments of the fraction of crypts with Paneth cells obtained from two methods are highly correlated (R^2=0.79, or correlation coefficient =0.89).

We used histology alone to analyze the timing of different pathologies, including crypt apoptosis and exfoliation to infer the contribution of each event to Paneth cell loss, since DKO ilea significantly lose Paneth cells at 27-day-old and completely at 35-day- old (Fig. 5D–F). The increase of crypt apoptosis coincides with the onset of Paneth cell loss; the Paneth cells are about half depleted by 28–29 days before the significant increase in crypt exfoliation at 31 days. Thus, we surmise that apoptosis contributes to 1/2- 2/3 of Paneth cell loss and exfoliation contributes to 1/3-1/2 of Paneth cell loss in the DKO mice. Because *Duoxa*-TKO ileum has virtually no elevated exfoliation, the

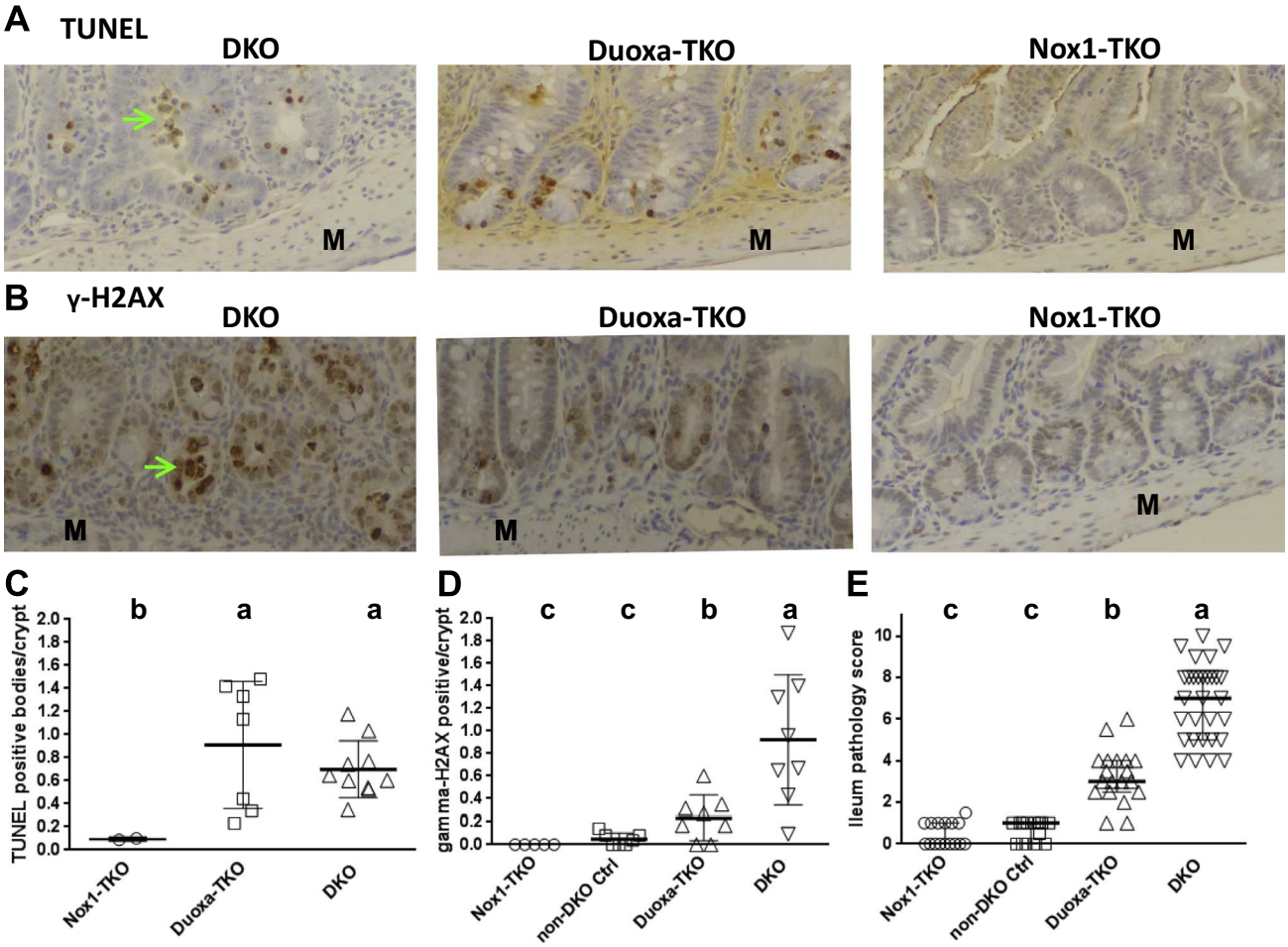

Fig. 3. *Duoxa*-TKO ileum has the same high level of TUNEL+ apoptotic cells as the DKO ileum but intermediate levels of DNA damage and pathology between DKO and *Nox1*-TKO mice. Panel A and B show IHC of TUNEL and anti-p-γH2AX Ab stained crypt. Panel C shows the counts of TUNEL+ cells per crypt ilea from 2 *Nox1*-TKO, 5 *Duoxa*-TKO and 5 DKO mice to validate the histology result. Non-DKO ileum is similar to *Nox1*-TKO, thus is not repeated here [9]. Panel D plots p-γH2AX+ cells per crypt from 5 *Nox1*-TKO, 7 non-DKO controls, 8 *Duoxa*-TKO and 8 DKO mice. The scoring excludes apparent apoptotic and exfoliated cells. Panel E shows ileum pathology score from 16 *Nox1*-TKO, 14 non-DKO controls, 19 Duoxa-TKO and 30 DKO mice. Bars indicate means ± SDs. Panel C and D are analyzed by pair-wise *t*-test and Panel E by 1-way ANOVA accounting for multiple comparisons (Dunnett's). Green arrows point out exfoliated cells.

partial loss of Paneth cells is likely contributed by apoptosis alone. Frank inflammation of DKO ilea occurs at 30 days of age as indicated by MPO+ cell infiltration and prominent crypt abscesses (reaching high levels after 30 days), coincident with the large increase in exfoliation incidence and the additional loss of Paneth cells (Fig. 5G, H).

The impact of DUOX2 in the colon of *Duoxa*-TKO mice is less evident since DKO mice have milder pathology in the colon than the ileum (Supplementary Fig. 4). A significant impact of DUOX2 inactivation was detected as decreased crypt apoptosis and exfoliation, while other scored parameters were unaffected. Similar to the ileum, T4 did not affect colon pathology (data not shown).

3.4. *Nox1* produces stronger oxidative stress than *Duox2* in the DKO intestine

ROS-induced DNA-stand breaks are associated with cellular apoptosis, and nuclear localization of γ-H2AX is a marker for double-strand DNA breaks [35]. As expected, the DKO ilea have a high level of γ-H2AX-positive foci (Fig. 3B, D). *Duoxa*-TKO ilea have 4-fold lower γ-H2AX-positive foci than DKO ilea, while non-DKO ilea and Nox1-TKO ilea have almost no γ-H2AX-positive foci. These results suggest that both Duox2 and Nox1 promote DNA breaks, and even a low level of DNA breaks can lead to apoptosis.

One marker for oxidative stress is *Hmox1* gene expression, which is induced by Nrf2, a transcription factor highly responsive to oxidative and electrophilic stresses [42]. We found *Hmox1* mRNA levels were low in the non-DKO control and Nox1-TKO mice and elevated to a similar level (5X and 7X) in the Duoxa-TKO and DKO mice (Fig. 6A). Taken together, these results suggest that Nox1 produced more oxidative stress than Duox2 in DKO ilea.

Since DKO ilea had sporadic increases of crypt apoptosis at 24–26 days of age, and DKO ilea have elevated *Nox1* expression compared to WT ilea [9], we also analyzed the developmental changes of *Nox1* expression. We found that *Nox1* mRNA levels gradually increased in post-weaning DKO ilea coincident with increased pathology, especially with crypt apoptosis (Fig. 5D–I). The elevated apoptosis is associated with elevated levels of *Nox1* mRNA within each age set. Presumably, the increase of ileal *Nox1* gene expression in the post-weaning DKO mice is due to changes in luminal microbe and diets.

3.5. Stronger DUOX2 activity may contribute to the more severe colitis in 129 DKO compared to B6 DKO mice

Duox2 is a top candidate gene in the *Gdac1* locus linked to milder inflammation severity in congenic 129 DKO mice carrying B6 *Gdac1* allele [43]. We explored whether the 129 *Duox2* allele had a higher intrinsic activity compared to the B6 allele to account for stronger inflammation in 129 DKO mice. To test this, four variants of *Duox2* cDNA were generated from B6 *Duox2* cDNA. Three variants had a single nucleotide change to carry each of non-synonymous codon

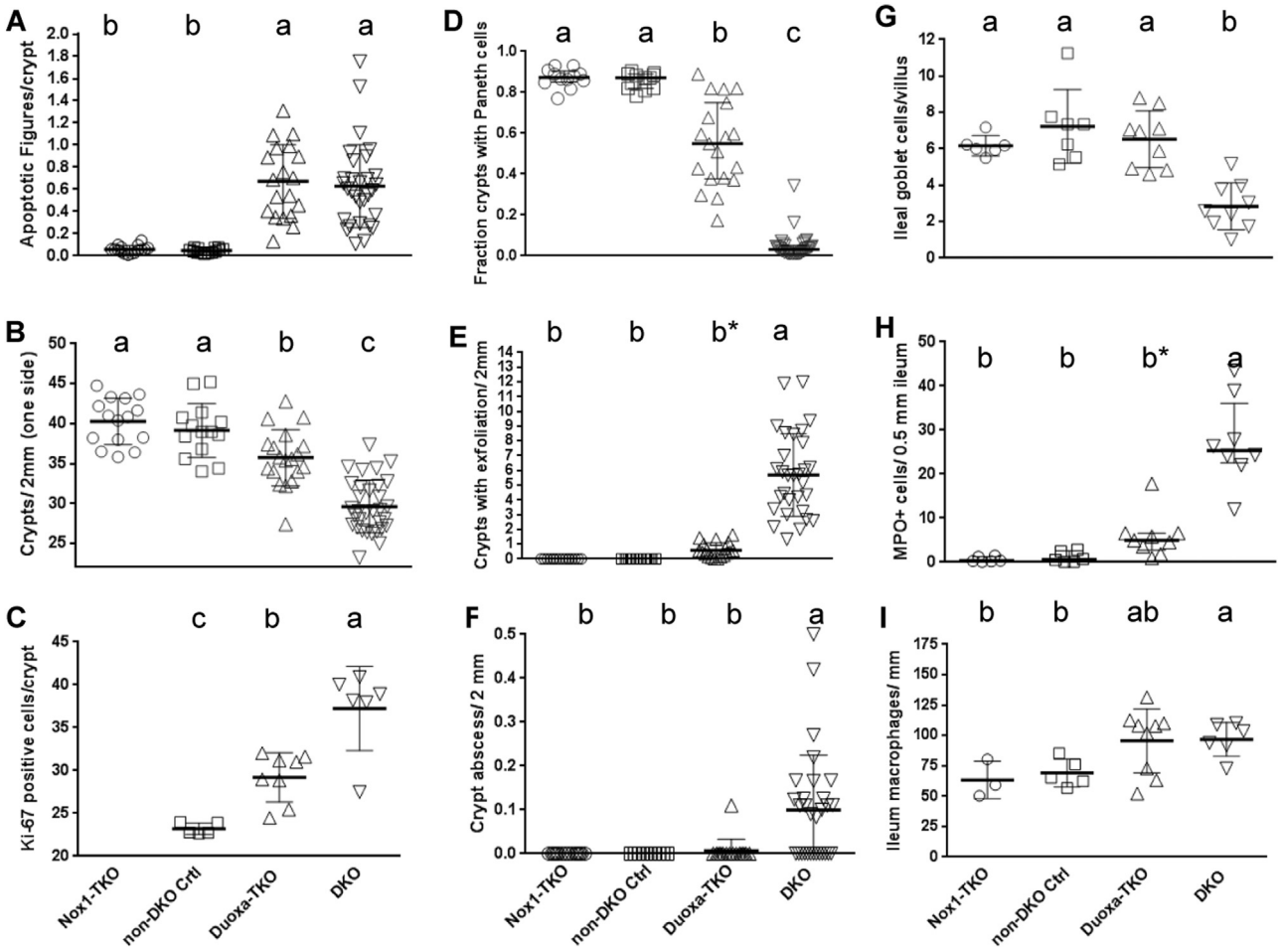

Fig. 4. *Duoxa*-TKO ilea have the same high level of crypt apoptotic figures as the DKO ilea but intermediate levels of crypt density, Paneth cells and proliferating cells between non-DKO and DKO mice. Panel A shows the number of apoptotic figures counted from H & E stained sections (see Table 1 for scoring method). Panel B shows crypt density and Panel C is Ki-67+ proliferating cells per ileum crypt. Panel D shows fraction of crypts with mature Paneth cells (containing eosinophilic granules). Panel E shows number of crypts with exfoliation per 2 mm (top, scoring both sides of tissue). Panel F shows the number of crypt abscesses (scored per 10X field from all tissue on the slide), analyzed by pair-wise *t*-tests. The mouse number in Panels A-F except the Ki-67 IHC is the same as that studied for total pathology score (Fig. 3E). The Ki-67 IHC was performed on 5 non-DKO control, 8 *Duoxa*-TKO and 6 DKO mice. Panel G shows the number of Alcian Blue+ cells per villus to crypt unit scored from 24 to 50 units analyzed from 6 *Nox1*-TKO, 7 non-DKO, 9 *Duoxa*-TKO and 9 DKO mice. Panel H shows the number of MPO+ cells in the submucosa (excluding crypt abscesses) per 0.5 mm ileum (one side) from 7 to 12 areas per mouse studied from 6 *Nox1*-TKO, 6 non-DKO, 9 *Duoxa*-TKO and 8 DKO mice. Panel I shows CD68+ cells (pan-macrophage marker) counts per 1 mm of the ileum (one side) averaged from 4 to 7 fields from 3 *Nox1*-TKO, 5 non-DKO controls, 9 *Duoxa*-TKO and 7 DKO mice. All figures except Paneth cell counts are shown as means ± SDs, and evaluated by 1-way ANOVA using DKO first then *Duoxa*-TKO as the reference. Paneth cell counts are shown as medians ± IQRs, and analyzed using Kruskal-Wallis test with DKO and *Duoxa*-TKO as reference sets. b* means that in pair-wise comparisons with the *Nox1*-TKO and non-DKO control, *Duoxa*-TKO exfoliation and MPO+ cells were significantly greater ($P < 0.001$).

substitutions (nsSNPs) corresponding to the 129 allele (i.e. A378G, V495D and H627R) and the 4th variant had all three nsSNPs (i.e. it encodes the 129 *Duox2* cDNA). The H627R variant and 129 allele had 1.6- and 7.6-fold higher activity than the B6 allele after activation by ionomycin and PMA, respectively (Supplementary Fig. 5A, 5B). The other two 129 variants, A378G and V495D, did not have higher activity than B6 allele. These results support the view that DUOX2 activity exacerbates redox imbalance and disease severity in DKO mice, which can be attributed primarily to the effects of the H627R SNP.

3.6. *Duoxa-TKO ilea have higher expression of Nox1 than DKO ilea to support crypt apoptosis*

Since *Nox1* and *Duox2* gene expression is elevated in inflamed intestine, we analyzed *Nox1* and *Duox2* gene expression in *Duoxa*-TKO and *Nox1*-TKO ilea respectively. Interestingly, *Nox1* mRNA levels are 2.5-fold higher in the *Duoxa*-TKO than DKO ilea, and *Duoxa2* mRNA levels are 2-fold higher in the *Nox1*-TKO than DKO and non-DKO control mice (Fig. 6B, D). This result, suggests that *Nox1* and *Duoxa2* gene expression is compensatory to each other. *Duox2* and *Nox2* gene expression was not altered in these mice and Nox4 was virtually undetectable in the ileum (Fig. 6C and data not shown). Nox1 is known as an executioner of Tnf-α-induced apoptosis after activation by riboflavin kinase, which forms a bridge between Tnfr1 death domain and p22phox subunit of Nox1 [44]. The high levels of *Tnf*-α mRNA, detected in *Duoxa*-TKO and DKO ilea supports the idea that the Nox1-mediated apoptosis is induced by *Tnf-α* (Fig. 6E).

Several matrix metalloproteinase (Mmp), such as Mmp-2, -3 and -9 are up-regulated in the intestines of IBD patients and may regulate epithelial barrier function [45,46]. Because the expression of these Mmps are associated with Nox1 and Duox1 [47–49], we analyzed the gene expression in our mice and found that *Mmp-2* and *Mmp-9*, but not *Mmp3* mRNA levels were significantly elevated in the DKO ilea compared with the non-DKO controls (Fig. 6F, G and data not shown). *Mmp-2* and *Mmp-9* mRNA levels in the *Duoxa*-TKO were slightly elevated over control levels with only *Mmp-9* levels reaching statistical significance.

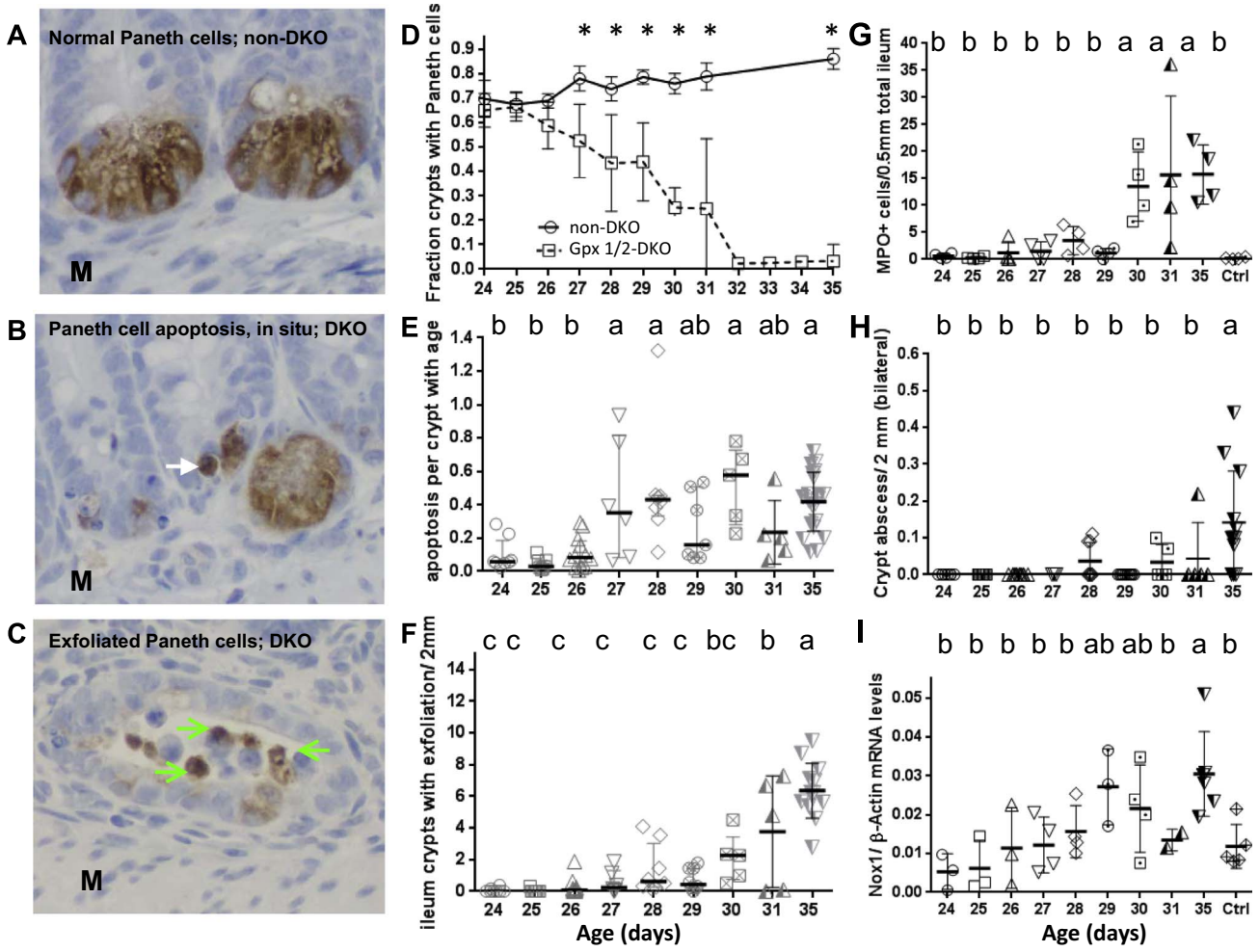

Fig. 5. Paneth cell apoptosis and exfoliation shown by anti-lysozyme Ab IHC and development of ileal pathology in the post-weaning DKO mice. Panel A shows the normal appearance of Paneth cells stained by anti-Lyz1 IHC in a non-DKO (*GPx1*$^{-/-}$*GPx2*$^{+/-}$) mouse (DAB substrate; hematoxylin counterstained). Panel B shows a putative apoptotic Paneth cell judging by shriveled Lys1+ appearance in the DKO crypt (pointed by a white arrow). Apoptotic Paneth cells, in situ, are also demonstrated in Supplementary Fig. 3 as double-stained Paneth cells with sequential TUNEL IHC (dark grey to black color stain) and anti-Lyz1 Ab IHC (red/brown stain). Panel C shows Lyz+ exfoliated cells (green arrows) in DKO crypt. Panel D shows that Paneth cell number begins to decline at 26 days and nearly depleted by 32-day-old. From 27 days on, the Paneth cell number is significantly lower in DKO compared to the control mice (*, one-way ANOVA test). The progression of the apoptosis pathology (Panel E), crypt exfoliation (Panel F), counts of MPO+ cells in the ileal submucosa (Panel G), appearance of ileum crypt abscesses (Panel H) and increase of *Nox1* mRNA levels (Panel I) were analyzed from the ileum of 24- to 35-day-old DKO mice. Two to four mice were analyzed for each day of DKO mice and 35-day-old non-DKO controls. All panels are shown as mean ± SD. Panel D, E, F and H were analyzed by histology. The numbers of non-DKO and DKO mice analyzed were 7, 8 of 24-day-old; 2, 7 of 25-day-old; 4, 12 of 26-day-old; 6 each of 27-day-old; 8 each of 28-day-old; 5, 7 of 29-day-old; 5 each of 30-day-old; 3, 5 of 31-day-old; and 14, 13 of 35-day-old, respectively. MPO IHC was done on 4 samples each and Nox1 qPCR on 2 to 4 samples at each time point. For Panel D the comparison is between the non-DKO and DKO at each age using *t*-test. In Panel E–H analysis is done by one-way ANOVA test using 24- to 35-day-old sets as reference sequentially against the remaining sets using Dunnett's multiple-correction test. Panel I was analyzed by pair-wise *t*-test.

3.7. Duoxa-TKO ilea have elevated expression of secretary cell markers than DKO ilea

We evaluated the levels of epithelial cell types by quantification of the mRNA levels of cell-specific markers using *Lyz1* for Paneth cells, *Muc2* for goblet cells and intestinal alkaline phosphatase (*Alpi*) for absorptive cells [50,51]. Consistent with Paneth cell counts, non-DKO control ilea had the highest *Lyz1* mRNA levels, whereas *Duxoa*-TKO and DKO ileum had about 50% and 24% of the control level (Fig. 6H). The magnitude of difference in the *Lyz1* mRNA between the DKO and non-DKO control is much less than the histological data (4.2-fold *Lyz1* mRNA vs. 24-fold for Paneth cell count by H & E and 9-fold by lysozyme IHC). *Duxoa*-TKO ilea had the same *Muc2* mRNA level as control mice and higher than that in the DKO mice (Fig. 6I). There was no difference in *Alpi* mRNA levels between groups (data not shown). The pattern of marker gene expression between groups is consistent with the result obtained by the morphological analysis.

3.8. DUOX2 is also expressed in the crypt epithelium of inflamed human colon biopsies

Duox2 protein expression is restricted to the apical surface of normal intestinal epithelium [3]. Since Duox2 affects crypt epithelial cell pathology in the DKO ileum, we suspect that Duox2 is also expressed in the inflamed crypt epithelium. Using a monoclonal anti-human DUOX Ab (which does not cross react with mouse Duox proteins), we detected abundant DUOX2 protein on the plasma membrane of the entire gland of colon biopsies isolated from colitis patients (Fig. 7). In the inflamed colon biopsies, many epithelial cells are stained at the apical and lateral surface of plasma membrane as well as intracellular perinuclear region along the entire gland axis. In the colon biopsies from normal-looking areas, very few epithelial cells are stained by the DUOX Ab, and the staining is present in both apical membrane and intracellular membranes as reported previously [38]. The expression of DUOX2 at the base of inflamed colon glands suggests that Duox2 can have a direct effect in crypt epithelium.

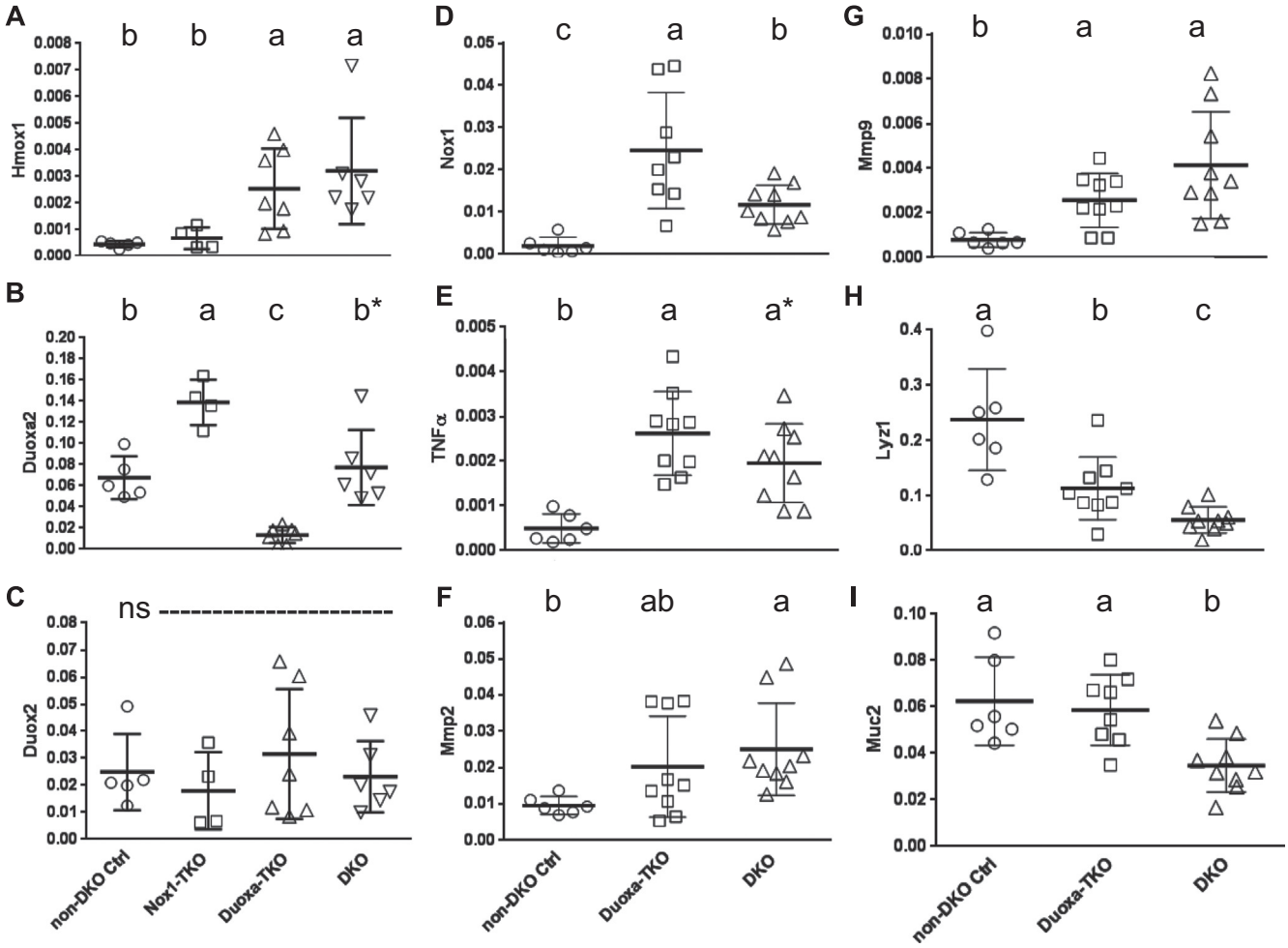

Fig. 6. The gene expression pattern in *Duoxa*-TKO ilea suggests the presence of oxidative stress. Panel A–C compare *Hmox1*, *Duoxa2* and *Duox2* mRNA levels among the non-DKO control, Nox1-TKO, Duoxa-TKO and DKO groups. Panel D–I show *Nox1*, *Tnfa*, *Mmp2*, *Mmp9*, *Lyz1* and *Muc2* mRNA levels between the non-DKO control, *Duoxa*-TKO and DKO groups. Horizontal bars are mean ± SD. Sample sizes for Panel A-C were 5 non-DKO controls, 4 *Nox1*-TKO, 7 *Duoxa*-TKO and 6 DKO. Sample sizes for panels D–I were 6 non-DKO; 9 *Duoxa*-TKO except 8 for Muc2 and Nox1 mRNA; and 9 DKO. All mRNA levels were normalized with *β-Actin*. Statistical analysis was performed by pair-wise *t*-tests. ns, not significant.

3.9. NOX inhibitors, DTI and THZ, as well as antioxidant MitoQ partially alleviated inflammation in the DKO mice

Gut inflammation in the DKO mice originates from deficiency in antioxidant enzymes, and removal of ROS-producing enzymes, NOX1 or DUOX2, ameliorates the inflammation. Thus, we tested the effect of NOX inhibitors and antioxidants on the DKO mice. Five of the eight antioxidants tested, DTI, celastrol, ebselen, GKT137831 and THZ inhibit NOXs in vitro or in cell lines (Table 2) [19,21,22,24,25,52]. Caffeic acid and deferoxamine are iron chelators. MitoQ is a mitochondria-targeted antioxidant [26–28].

Among the eight compounds tested, only two NOX inhibitors, oral DTI (5/10 mice treated with score of ≤4) and THZ (9/20 treated with score of ≤4), as well as MitoQ (9/21 treated with score of ≤4) significantly lowered DKO ileal pathology scores (Fig. 8A). A drug decreasing DKO pathology scores to 4 or below is considered efficacious, since only 2/35 non-treated DKO and 17/19 non-treated *Duoxa*-TKO mice have a score of ≤4. Clearly, the drug effect was mild compared to that by genetic inactivation of Nox1 or Duox2. Because Nox1 drives crypt apoptosis in the DKO ileum, and half of the mice responding to DTI (IP plus oral) had fewer apoptotic figures in the crypts, this result suggests that the DTI effect is mediated by Nox1 inhibition (Fig. 8B). DTI did not affect *Nox1* mRNA levels in the DKO ilea (data not shown), not supporting DTI's inhibition of NOX1 mRNA levels in colon cancer LS-174T cells [21]. In terms of NOX-promoted Paneth cell depletion, DTI and MitoQ blunted the loss of Paneth cells (Fig. 8C). DTI (both oral and i.p treated), MitoQ and THZ partially blocked loss of crypts, similar to Duox2 deficiency (Fig. 8D). Most impressively, MitoQ also dampened crypt exfoliation (Fig. 8E). This may be significant since mitochondria integrate signals from focal adhesions in the initiation of apoptosis [53]. However, none of the compounds affected crypt abscesses (Fig. 8F). Deferoxamine mesylate-treated mice (N=7) did not show any improvement (data not shown).

In view of the mild colitis observed in the DKO mice, none of the compounds tested improved colon pathology when analyzed collectively (Supplementary Fig. 4G, 4H). Nonetheless, a subset of mice responded to i.p. DTI (2/25 mice) and MitoQ (4/21 mice) as revealed by low-pathology scores. These same mice responded to DTI, MitoQ and THZ had lower levels of gland apoptosis.

4. Discussion

In this study, we demonstrated that *Duox2* expression is also associated with gut pathology in the DKO mice. *Nox1*, but not *Duox2*, has a strong impact on apoptosis of crypt epithelium. The Nox1 effect on apoptosis could be mediated through TNF activation of TNF receptor 1 (TNFR1) and riboflavin kinase, which forms a bridge between the RNFR1 death domain and the Cyba (a subunit of Nox1 enzyme) [44]. Additionally, the Nox1 expression can cause DNA damage leading to accumulation of γH2AX foci at DNA breakage sites [35]. ROS-associated DNA damage is unlikely to be driven by Fenton chemistry since deferoxamine, an iron chelator, does not affect

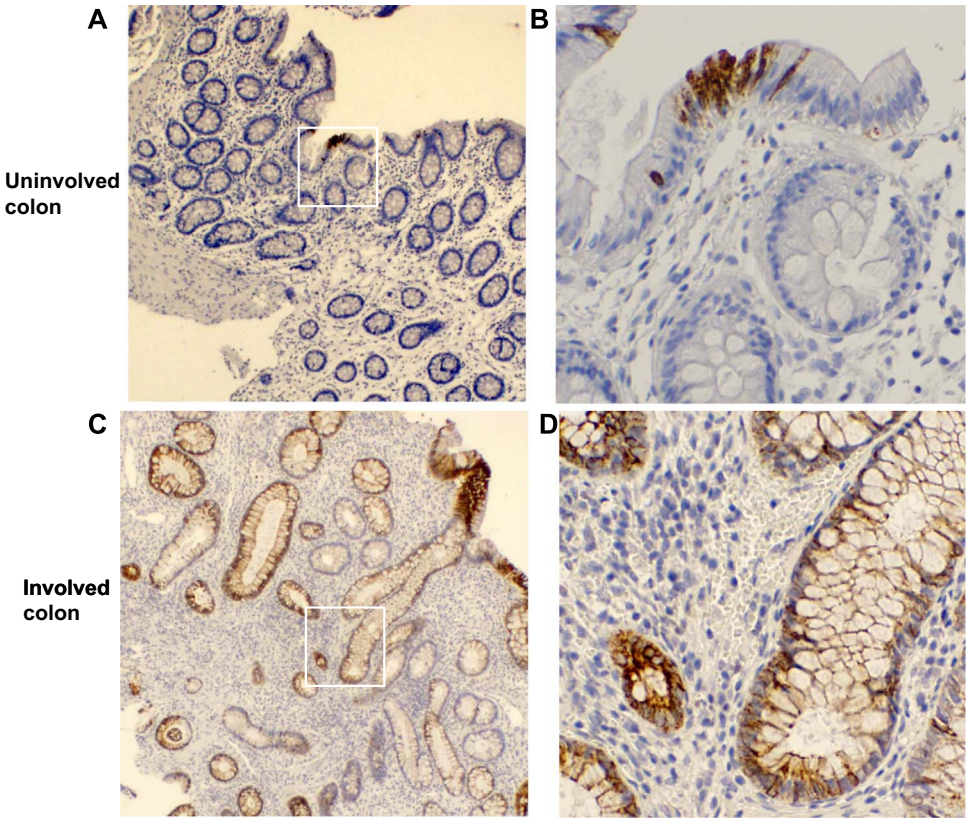

Fig. 7. The involved colon has higher levels of DUOX protein than uninvolved area from biopsies of colitis patients detected by IHC. Panel A and C are DUOX IHC of uninvolved and involved colon samples isolated from the same patient (40×, original magnification). The positive stain is shown in brown color. The white squares are enlarged in Panel B and D (200×, original magnification). The inflamed colon has more epithelial cells stained in the plasma membrane at apical, lateral and perinuclear areas. Similar results are obtained from five patients.

apoptosis. Therefore, Nox1 can induce cell apoptosis in addition to cell proliferation and migration in gut epithelial cells as shown by others [54]. The intestinal crypt epithelium of the DKO mice may be prone to oxidative stress, and GPx2 plays a critical role to protect crypt epithelial cells from apoptosis [32].

Apoptosis in crypt epithelial cells is a hallmark of IBD pathology and it is thought to contribute to inflammation [55]. However, as demonstrated in *Duoxa*-TKO ilea with high levels of crypt apoptosis, these mice had a normal growth and didn't have crypt epithelium exfoliation. It suggests that epithelial cell exfoliation is a better marker for inflammation. Exfoliation contributes to significant loss of Paneth cells in the DKO ilea. Paneth cells secrete antimicrobial factors (e.g. cryptidins and phospholipase A_2) that limit bacterial penetration into mucosa [14]. Exfoliation of Paneth cells leading to profound depletion was also reported in rat jejunum after I/R stress [56]. Furthermore, Duox2 inactivation also enhanced Muc2 expression, similar to the effect of Nox1 deficiency in the WT mice [9,57]. Muc2 can form a barrier to prevent luminal bacteria contacting the mucosal epithelium to prevent infection or inflammation [58]. Hence, the higher numbers of goblet and Paneth cells in the *Duoxa*-TKO ilea than the DKO ilea protect them from inflammation.

Crypt abscesses, infiltration of MPO+ cells into the submucosa and epithelial exfoliation remain good markers for inflammation. The abscessed crypts contain neutrophils with engulfed microbes, and exfoliated epithelium has probably been invaded by pathogens [59]. During the development of inflammation in the DKO mice, exfoliation and infiltration of MPO+ cells increases greatly after 29 days of age, lagging behind Paneth cell loss and crypt apoptosis (26–27 days). This sequence of events supports the idea that crypt apoptosis leads to Paneth cell loss. When coupled with partial loss of goblet cells which weakens host antibacterial defense, Paneth cell loss allows bacterial invasion into the mucosa triggering a full-blown inflammatory response.

Although *Duoxa*-TKO ilea do not exhibit inflammatory pathology, they have elevated levels of *Tnfα*, a pro-inflammatory cytokine mRNA expression similar to DKO ilea and higher levels of *Nox1* expression than the DKO ilea. Because *Nox1*-TKO ileum does not have elevated TNF-α levels [9], we suspect that the high crypt apoptosis in the *Duoxa*-TKO mice causes slight leakiness, which exposes mucosa to luminal microbial products and increases cytokine production. Mice without Duox2 activity have higher mucosal bacterial intake [5]. This is consistent with the idea that Duox2 plays an essential role in antibacterial defense. The presence of DUOX2 in the base of colitis colon epithelium suggests that it acts locally.

Duoxa-TKO ilea had elevated *Nox1* gene expression. It is possible that *Duoxa*-TKO ilea have faster cell proliferation from the crypt epithelium, where Nox1 is expressed [54]. It is also possible that Duox2 and Nox1 have compensatory activities with overlapping functions to defend against bacterial invasion. Some of the oxidase effects are mediated through activation of Mmp proteins, and activation of Mmp-2 can maintain epithelial barrier function [46].

Previously, using classic genetic mapping, we identified the *Gdac1* locus, which modifies disease severity in the DKO mice [43,60]. The 129-*Gdac1*^{B6} congenic DKO mice containing the B6 allele show moderate disease compared to the aggressive disease in 129 DKO mice. *Duox2* is a top candidate gene residing in this locus. Here we show that 129 Duox2 allele has indeed higher in vitro activity than the B6 allele, consistent with our data in *Duoxa*-TKO mice indicating a possible role of Duox2-associated oxidative stress in intestinal redox imbalance of DKO mice.

Redox imbalance may increase susceptibility to IBD. ROS generated by NOX enzymes play an important role in IBD pathogenesis,

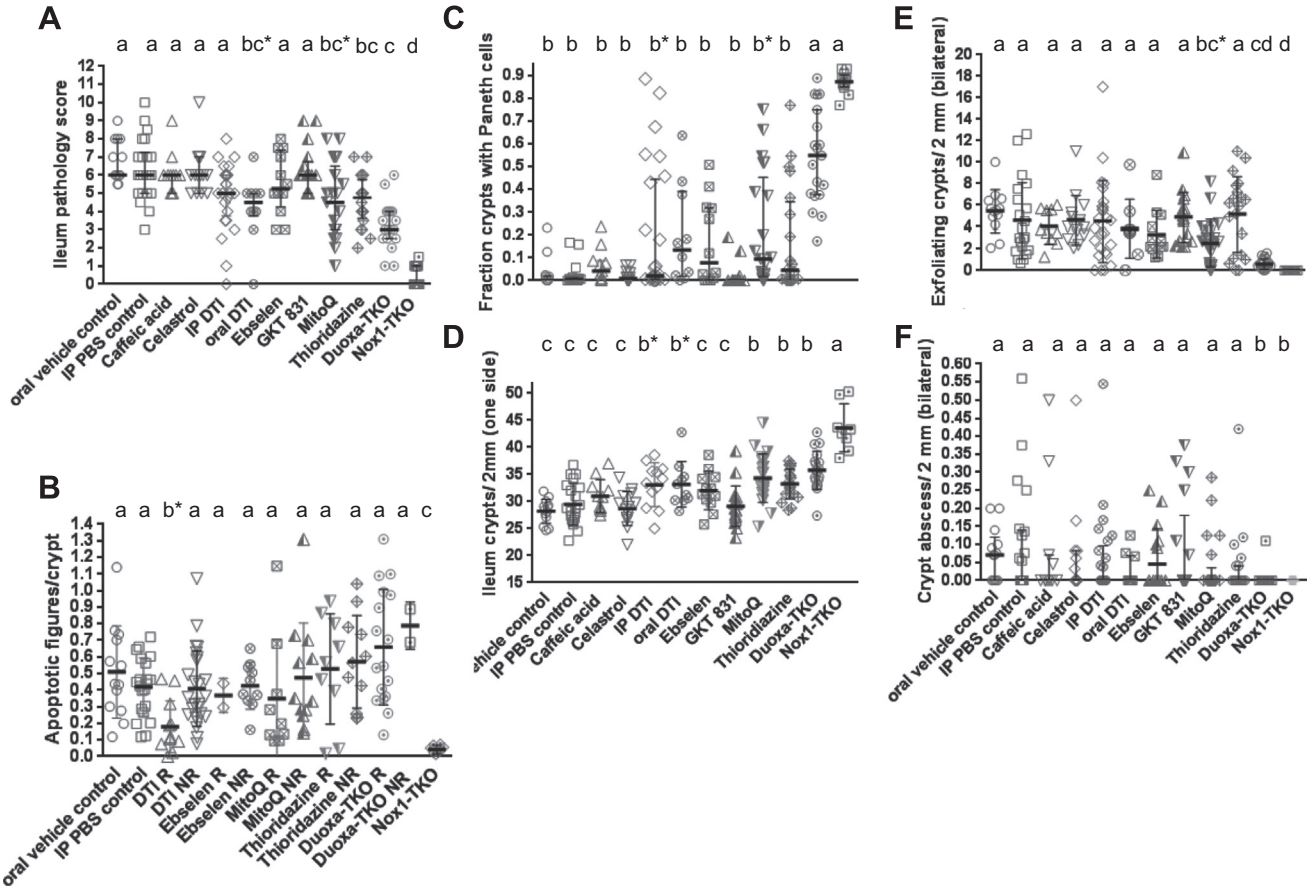

Fig. 8. DTI and THZ, two small molecule NOX inhibitors and MitoQ antioxidants have efficacy on DKO ileal pathologies. Drugs were tested on the DKO mice; the oral vehicle-treated *Duoxa*-TKO and *Nox1*-TKO groups were repeated here for reference. Panel A shows pathology scores as median ± IQR (Kruskal-Wallis test; Primary analysis against oral and intraperitoneal (IP) PBS controls). Groups marked by asterisks were significantly different from the oral-vehicle control but not the IP-PBS control. Panel B shows the drug effect on apoptotic figure per crypt from the subgroups that show significant decrease in total pathology, i.e. DTI (pooling oral and i.p. sets), ebselen, MitoQ and THZ. These subgroups were stratified into responding (R; with pathology score ≤4) and non-responding (NR) groups shown as mean ± SD. Only DTI-R group has less apoptosis (b*) than DKO treated with oral vehicle but not the IP-PBS control (1-way ANOVA using DKO controls as reference). Pair-wise comparison showed that DTI-R had less apoptosis than IP-PBS control (P=0.0005) and the NR set (P=0.0032). Panel C shows significant drug effect on Paneth cell loss (median ± IQR; Kruskal-Wallis test). b* means that the set was not distinguishable from the *Duoxa*-TKO set in a multiple-comparisons test, but it is different by pair-wise comparison. Panel D shows drug effect on crypt density (mean ± SD). b* indicates that the set has a higher density than the oral vehicle control, but not the IP-PBS control (1-way ANOVA). Panel E shows drug effect on crypt exfoliation (median ± IQR). bc* indicates that the MitoQ groups was different from the oral-control but not the IP-control groups. Panel F shows no drug effect on crypt abscesses (median ± IQR, Kurskal-Wallis using both control sets as references). The numbers of mice studied are 13 oral-vehicle control, 22 IP-PBS control, 11 caffeic acid, 14 celastrol, 25 IP-DTI, 10 oral-DTI, 12 ebselen, 17 GKT137831/GKT 831, 21 MitoQ and 20 THZ DKO, as well as 19 *Duoxa*-TKO and 16 *Nox1*-TKO.

especially in VEO-IBD [61,62]. The phagocytic NOX2 complex consists of six subunits, two transmembrane subunits, NOX2/gp91phox/CYBB and p22pox/CYBA, as well as four cytosolic subunits, p47phox/NCF1, p67phox/NCF2, p40phox/NCF4 and a small GTPase (RAC1 or RAC2) to activate the enzyme complex [63]. The activated NOX2 complex in neutrophils releases ROS into phagosomes to kill endocytosed bacteria [64]. Mutations in NOX2, NCF1, and NCF2 are noted in patients with IBD-like pathology or VEO-IBD (diagnosed before 6 years of age) [65]. DUOX2 and NOX1 variants are associated with VEO-IBD patients who demonstrate lower activity than healthy controls [62]. However, DUOX2 and DUOXA2 expression were induced up to 16- and 52-fold, respectively, in pediatric and adult Crohn's disease patients [6,7]. Because the DKO mice develop VEO-IBD-like disease, this model could prove to be an invaluable tool for the study of the effects of NOX inhibitors or the development of other therapeutic modalities against this difficult-to-treat VEO-IBD.

Because the IBD pathology in the DKO mice is dependent on *Nox1* or *Duox2* expression, we evaluated the efficacy of NOX inhibitors and antioxidants in our DKO mouse model. Two NOX inhibitors, DTI and THZ, as well as MitoQ have efficacy in decreasing inflammation. DTI is less toxic than diphenylene iodonium (DPI) to DKO mice; it inhibits NOX1 much better than DUOX2 [21]. A fraction (9 of 38) of DTI-treated DKO mice had significantly decreased crypt apoptosis (apoptosis/crypt ≤0.12), suggesting that the drug reaches crypts to inhibit NOX1 activity. Due to DTI-induced morbidity in a small number of mice, it is not a likely candidate for clinical testing. DTI analogs show potential for drug development with reduced toxicity. THZ (Orsanil™), an N-substituted phenothiazine derivative, is an anthelmintic and antipsychotic drug and inhibits all NOXs and DUOX2 [25](data not shown). Since the dose that we used had an adverse sedative effect prohibiting dose escalation, other analogs need to be tested for efficacy and developed into therapeutic drugs.

MitoQ is a lipophilic triphenylphosphonium (TPP) cation that can permeate lipid bilayers and accumulates in the mitochondria. MitoQ protects mice from dextran sulfate sodium-induced colitis [26]. The MitoQ effect is similar to, although more modest than DUOX2-inactivation, i.e. no effect on apoptosis, partial retention of Paneth cells and crypt density and decrease in exfoliation. The impact on anoikis appears to confirm the central role of mitochondria in the integration of a death signal from the extracellular matrix [66]. Perhaps MitoQ may have efficacy in human IBD therapy.

In this study, we have demonstrated that *Duox2* contributes to gut pathology in the DKO mice. A striking difference between *Nox1*- and *Duoxa*-TKO is crypt apoptosis, which is largely contributed by Nox1.

Since ROS-generating enzymes including NOX1 and DUOX2 have been associated with VEO-IBD, NOX inhibitors may in the future play a role in the treatment of VEO-IBD. DKO mice provide an excellent model for screening NOX1 and DUOX2 inhibitors that might have a therapeutic role for patients with VEO-IBD.

Author contributions

RSE, JHD and FFC provided study concept and design; RSE and FFC acquired data for most part, analyzed and interpreted the data, and drafted the manuscript. AD and TLL acquired data for *Duox2* alleles, HG, JHD and TLL critically revised the manuscript. JHD, HG and GQ provided material support and JHD and BS obtained funding support.

Disclosure

The authors declared no conflict of interest.

Grant support

Supported by Federal funds from the National Cancer Institute (NCI) under Contract No. HHSN261200800001E and funds from the intramural research program of National Institute of Allergy and Infectious Diseases. Research reported in this publication included work performed in the Anatomic Pathology and Animal Resource Cores supported by the NCI of the National Institutes of Health under award number P30CA33572 to City of Hope. The content of this publication does not necessarily reflect the views of policies of the Department of the Health and Human Services, nor does mention of trade names, commercial products, or organizations imply endorsement by the US Government.

Acknowledgements

We thank Cedric Szyndralewiez at GenKyoTex, Geneva, Switzerland for providing GKT 137831 and its formulation for this study and Tina Montgomery of the Anatomical Pathology core, City of Hope, for excellent technical support of the histology and IHC projects.

Appendix A. Supporting information

Supplementary data associated with this article can be found in the online version at doi:10.1016/j.redox.2016.11.001.

References

[1] A. Bhattacharyya, R. Chattopadhyay, S. Mitra, S.E. Crowe, Oxidative stress: an essential factor in the pathogenesis of gastrointestinal mucosal diseases, Physiol. Rev. 94 (2014) 329–354.
[2] Y.A. Suh, R.S. Arnold, B. Lassegue, J. Shi, X. Xu, D. Sorescu, A.B. Chung, K.K. Griendling, J.D. Lambeth, Cell transformation by the superoxide-generating oxidase Mox1, Nature 401 (1999) 79–82.
[3] R.A. El Hassani, N. Benfares, B. Caillou, M. Talbot, J.C. Sabourin, V. Belotte, S. Morand, S. Gnidehou, D. Agnandji, R. Ohayon, J. Kaniewski, M.S. Noel-Hudson, J.M. Bidart, M. Schlumberger, A. Virion, C. Dupuy, Dual oxidase2 is expressed all along the digestive tract, Am. J. Physiol. Gastrointest. Liver Physiol. 288 (2005) G933–G942.
[4] F. Sommer, F. Backhed, The gut microbiota engages different signaling pathways to induce Duox2 expression in the ileum and colon epithelium, Mucosal Immunol. 8 (2015) 372–379.
[5] H. Grasberger, J. Gao, H. Nagao-Kitamoto, S. Kitamoto, M. Zhang, N. Kamada, K.A. Eaton, M. El-Zaatari, A.B. Shreiner, J.L. Merchant, C. Owyang, J.Y. Kao, Increased expression of DUOX2 is an epithelial response to mucosal dysbiosis required for immune homeostasis in mouse intestine, Gastroenterology 149 (2015) 1849–1859.
[6] Y. Haberman, T.L. Tickle, P.J. Dexheimer, M.O. Kim, D. Tang, R. Karns, R.N. Baldassano, J.D. Noe, J. Rosh, J. Markowitz, M.B. Heyman, A.M. Griffiths, W.V. Crandall, D.R. Mack, S.S. Baker, C. Huttenhower, D.J. Keljo, J.S. Hyams, S. Kugathasan, T.D. Walters, B. Aronow, R.J. Xavier, D. Gevers, L.A. Denson, Pediatric Crohn disease patients exhibit specific ileal transcriptome and microbiome signature, J. Clin. Invest. 124 (2014) 3617–3633.
[7] T.S. MacFie, R. Poulsom, A. Parker, G. Warnes, T. Boitsova, A. Nijhuis, N. Suraweera, A. Poehlmann, J. Szary, R. Feakins, R. Jeffery, R.W. Harper, A.M. Jubb, J.O. Lindsay, A. Silver, DUOX2 and DUOXA2 form the predominant enzyme system capable of producing the reactive oxygen species H2O2 in active ulcerative colitis and are modulated by 5-aminosalicylic acid, Inflamm. Bowel Dis. 20 (2014) 514–524.
[8] R. Carey, I. Jurickova, E. Ballard, E. Bonkowski, X. Han, H. Xu, L.A. Denson, Activation of an IL-6:STAT3-dependent transcriptome in pediatric-onset inflammatory bowel disease, Inflamm. Bowel Dis. 14 (2008) 446–457.
[9] R.S. Esworthy, B.W. Kim, J. Chow, B. Shen, J.H. Doroshow, F.F. Chu, Nox1 causes ileocolitis in mice deficient in glutathione peroxidase-1 and -2, Free Radic. Biol. Med. 68 (2014) 315–325.
[10] H. Grasberger, X. De Deken, O.B. Mayo, H. Raad, M. Weiss, X.H. Liao, S. Refetoff, Mice deficient in dual oxidase maturation factors are severely hypothyroid, Mol. Endocrinol. 26 (2012) 481–492.
[11] R.H. Siggers, D.J. Hackam, The role of innate immune-stimulated epithelial apoptosis during gastrointestinal inflammatory diseases, Cell Mol. Life Sci. 68 (2011) 3623–3634.
[12] C. Gunther, H. Neumann, M.F. Neurath, C. Becker, Apoptosis, necrosis and necroptosis: cell death regulation in the intestinal epithelium, Gut (2012).
[13] R. Kiesslich, C.A. Duckworth, D. Moussata, A. Gloeckner, L.G. Lim, M. Goetz, D.M. Pritchard, P.R. Galle, M.F. Neurath, A.J. Watson, Local barrier dysfunction identified by confocal laser endomicroscopy predicts relapse in inflammatory bowel disease, Gut 61 (2012) 1146–1153.
[14] S. Vaishnava, C.L. Behrendt, A.S. Ismail, L. Eckmann, L.V. Hooper, Paneth cells directly sense gut commensals and maintain homeostasis at the intestinal host-microbial interface, Proc. Natl. Acad. Sci. USA 105 (2008) 20858–20863.
[15] S. Altenhofer, K.A. Radermacher, P.W. Kleikers, K. Wingler, H.H. Schmidt, Evolution of NADPH oxidase inhibitors: selectivity and mechanisms for target engagement, Antioxid. Redox Signal. (2014).
[16] M.H. Omar, W. Mullen, A. Stalmach, C. Auger, J.M. Rouanet, P.L. Teissedre, S.T. Caldwell, R.C. Hartley, A. Crozier, Absorption, disposition, metabolism, and excretion of [3-(14)C]caffeic acid in rats, J. Agric. Food Chem. 60 (2012) 5205–5214.
[17] J. Zhang, C.Y. Li, M.J. Xu, T. Wu, J.H. Chu, S.J. Liu, W.Z. Ju, Oral bioavailability and gender-related pharmacokinetics of celastrol following administration of pure celastrol and its related tablets in rats, J. Ethnopharmacol. 144 (2012) 195–200.
[18] G. Chen, X. Zhang, M. Zhao, Y. Wang, X. Cheng, D. Wang, Y. Xu, Z. Du, X. Yu, Celastrol targets mitochondrial respiratory chain complex I to induce reactive oxygen species-dependent cytotoxicity in tumor cells, BMC Cancer 11 (2011) 170.
[19] S.M. Smith, J. Min, T. Ganesh, B. Diebold, T. Kawahara, Y. Zhu, J. McCoy, A. Sun, J.P. Snyder, H. Fu, Y. Du, I. Lewis, J.D. Lambeth, Ebselen and congeners inhibit NADPH oxidase 2-dependent superoxide generation by interrupting the binding of regulatory subunits, Chem. Biol. 19 (2012) 752–763.
[20] N.K. Dutta, M.L. Pinn, M. Zhao, M.A. Rudek, P.C. Karakousis, Thioridazine lacks bactericidal activity in an animal model of extracellular tuberculosis, J. Antimicrob. Chemother. 68 (2013) 1327–1330.
[21] J.H. Doroshow, S. Gaur, S. Markel, J. Lu, J. van Balgooy, T.W. Synold, B. Xi, X. Wu, A. Juhasz, Effects of iodonium-class flavin dehydrogenase inhibitors on growth, reactive oxygen production, cell cycle progression, NADPH oxidase 1 levels, and gene expression in human colon cancer cells and xenografts, Free Radic. Biol. Med. 57 (2013) 162–175.
[22] V. Jaquet, J. Marcoux, E. Forest, K.G. Leidal, S. McCormick, Y. Westermaier, R. Perozzo, O. Plastre, L. Fioraso-Cartier, B. Diebold, L. Scapozza, W.M. Nauseef, F. Fieschi, K.H. Krause, K. Bedard, NOX NADPH oxidase isoforms are inhibited by celastrol with a dual mode of action, Br. J. Pharmacol. (2011).
[23] H.Y. Li, J. Zhang, L.L. Sun, B.H. Li, H.L. Gao, T. Xie, N. Zhang, Z.M. Ye, Celastrol induces apoptosis and autophagy via the ROS/JNK signaling pathway in human osteosarcoma cells: an in vitro and in vivo study, Cell Death Dis. 6 (2015) e1604.
[24] J.X. Jiang, X. Chen, N. Serizawa, C. Szyndralewiez, P. Page, K. Schroder, R.P. Brandes, S. Devaraj, N.J. Torok, Liver fibrosis and hepatocyte apoptosis are attenuated by GKT137831, a novel NOX4/NOX1 inhibitor in vivo, Free Radic. Biol. Med. 53 (2012) 289–296.
[25] T. Seredenina, G. Chiriano, A. Filippova, Z. Nayernia, Z. Mahiout, L. Fioraso-Cartier, O. Plastre, L. Scapozza, K.H. Krause, V. Jaquet, A subset of N-substituted phenothiazines inhibits NADPH oxidases, Free Radic. Biol. Med. 86 (2015) 239–249.
[26] A. Dashdorj, K.R. Jyothi, S. Lim, A. Jo, M.N. Nguyen, J. Ha, K.S. Yoon, H.J. Kim, J.H. Park, M.P. Murphy, S.S. Kim, Mitochondria-targeted antioxidant MitoQ ameliorates experimental mouse colitis by suppressing NLRP3 inflammasome-mediated inflammatory cytokines, BMC Med. 11 (2013) 178.
[27] T.C. Genaro-Mattos, A.Q. Mauricio, D. Rettori, A. Alonso, M. Hermes-Lima, Antioxidant activity of caffeic acid against iron-induced free radical generation–a chemical approach, PLoS One 10 (2015) e0129963.
[28] G.M. Brittenham, Iron-chelating therapy for transfusional iron overload, N. Engl. J. Med. 364 (2011) 146–156.
[29] G. Gavazzi, B. Banfi, C. Deffert, L. Fiette, M. Schappi, F. Herrmann, K.H. Krause, Decreased blood pressure in NOX1-deficient mice, FEBS Lett. 580 (2006) 497–504.
[30] R.S. Esworthy, J.R. Mann, M. Sam, F.F. Chu, Low glutathione peroxidase activity in Gpx1 knockout mice protects jejunum crypts from gamma-irradiation damage, Am. J. Physiol. Gastrointest. Liver Physiol. 279 (2000) G426–G436.
[31] R.S. Esworthy, R. Aranda, M.G. Martin, J.H. Doroshow, S.W. Binder, F.F. Chu, Mice with combined disruption of Gpx1 and Gpx2 genes have colitis, Am. J. Physiol. Gastrointest. Liver Physiol. 281 (2001) G848–G855.

[32] S. Florian, S. Krehl, M. Loewinger, A. Kipp, A. Banning, S. Esworthy, F.F. Chu, R. Brigelius-Flohe, Loss of GPx2 increases apoptosis, mitosis, and GPx1 expression in the intestine of mice, Free Radic. Biol. Med. 49 (2010) 1694–1702.
[33] R.S. Esworthy, D.D. Smith, F.F. Chu, A strong impact of genetic background on gut microflora in mice, Int. J. Inflamm. 986046 (2010) 2010.
[34] R.S. Esworthy, B.W. Kim, G.P. Larson, M.L. Yip, D.D. Smith, M. Li, F.F. Chu, Colitis locus on chromosome 2 impacting the severity of early-onset disease in mice deficient in GPX1 and GPX2, Inflamm. Bowel Dis. 17 (2011) 1373–1386.
[35] M. Geric, G. Gajski, V. Garaj-Vrhovac, Gamma-H2AX as a biomarker for DNA double-strand breaks in ecotoxicology, Ecotoxicol. Environ. Saf. 105 (2014) 13–21.
[36] Y. Wu, S. Antony, S.M. Hewitt, G. Jiang, S.X. Yang, J.L. Meitzler, A. Juhasz, J. Lu, H. Liu, J.H. Doroshow, K. Roy, Functional activity and tumor-specific expression of dual oxidase 2 in pancreatic cancer cells and human malignancies characterized with a novel monoclonal antibody, Int. J. Oncol. 42 (2013) 1229–1238.
[37] R.A. Gioscia-Ryan, T.J. LaRocca, A.L. Sindler, M.C. Zigler, M.P. Murphy, D.R. Seals, Mitochondria-targeted antioxidant (MitoQ) ameliorates age-related arterial endothelial dysfunction in mice, J. Physiol. 592 (2014) 2549–2561.
[38] A. Donko, S. Morand, A. Korzeniowska, H.E. Boudreau, M. Zana, L. Hunyady, M. Geiszt, T.L. Leto, Hypothyroidism-associated missense mutation impairs NADPH oxidase activity and intracellular trafficking of Duox2, Free Radic. Biol. Med. 73 (2014) 190–200.
[39] K.K. Patel, H. Miyoshi, W.L. Beatty, R.D. Head, N.P. Malvin, K. Cadwell, J.L. Guan, T. Saitoh, S. Akira, P.O. Seglen, M.C. Dinauer, H.W. Virgin, T.S. Stappenbeck, Autophagy proteins control goblet cell function by potentiating reactive oxygen species production, EMBO J. 32 (2013) 3130–3144.
[40] G. Leoni, A. Alam, P.A. Neumann, J.D. Lambeth, G. Cheng, J. McCoy, R.S. Hilgarth, K. Kundu, N. Murthy, D. Kusters, C. Reutelingsperger, M. Perretti, C.A. Parkos, A.S. Neish, A. Nusrat, Annexin A1, formyl peptide receptor, and NOX1 orchestrate epithelial repair, J. Clin. Invest. 123 (2013) 443–454.
[41] M. Geiszt, J. Witta, J. Baffi, K. Lekstrom, T.L. Leto, Dual oxidases represent novel hydrogen peroxide sources supporting mucosal surface host defense, FASEB J. 17 (2003) 1502–1504.
[42] M.C. Lu, J.A. Ji, Z.Y. Jiang, Q.D. You, The Keap1-Nrf2-ARE pathway as a potential preventive and therapeutic target: an update, Med. Res. Rev. 36 (2016) 924–963.
[43] R.S. Esworthy, B.W. Kim, G.E. Rivas, T.L. Leto, J.H. Doroshow, F.F. Chu, Analysis of candidate colitis genes in the gdac1 locus of mice deficient in glutathione peroxidase-1 and -2, PLoS One 7 (2012) e44262.
[44] B. Yazdanpanah, K. Wiegmann, V. Tchikov, O. Krut, C. Pongratz, M. Schramm, A. Kleinridders, T. Wunderlich, H. Kashkar, O. Utermohlen, J.C. Bruning, S. Schutze, M. Kronke, Riboflavin kinase couples TNF receptor 1 to NADPH oxidase, Nature 460 (2009) 1159–1163.
[45] P. Garg, M. Vijay-Kumar, L. Wang, A.T. Gewirtz, D. Merlin, S.V. Sitaraman, Matrix metalloproteinase-9-mediated tissue injury overrides the protective effect of matrix metalloproteinase-2 during colitis, Am. J. Physiol. Gastrointest. Liver Physiol. 296 (2009) G175–G184.
[46] S. O'Sullivan, J.F. Gilmer, C. Medina, Matrix metalloproteinases in inflammatory bowel disease: an update, Mediat. Inflamm. 2015 (2015) 964131.
[47] P. Spallarossa, P. Altieri, S. Garibaldi, G. Ghigliotti, C. Barisione, V. Manca, P. Fabbi, A. Ballestrero, C. Brunelli, A. Barsotti, Matrix metalloproteinase-2 and -9 are induced differently by doxorubicin in H9c2 cells: the role of MAP kinases and NAD(P)H oxidase, Cardiovasc. Res. 69 (2006) 736–745.
[48] S. Xu, A.S. Shriver, D.K. Jagadeesha, A.H. Chamseddine, K. Szocs, N.L. Weintraub, K.K. Griendling, R.C. Bhalla, F.J. Miller Jr., Increased expression of Nox1 in neointimal smooth muscle cells promotes activation of matrix metalloproteinase-9, J. Vasc. Res. 49 (2012) 242–248.
[49] D.H. Choi, J.H. Kim, J.H. Seo, J. Lee, W.S. Choi, Y.S. Kim, Matrix metalloproteinase-3 causes dopaminergic neuronal death through Nox1-regenerated oxidative stress, PLoS One 9 (2014) e115954.
[50] A. Kaser, A.H. Lee, A. Franke, J.N. Glickman, S. Zeissig, H. Tilg, E.E. Nieuwenhuis, D.E. Higgins, S. Schreiber, L.H. Glimcher, R.S. Blumberg, XBP1 links ER stress to intestinal inflammation and confers genetic risk for human inflammatory bowel disease, Cell 134 (2008) 743–756.
[51] M.A. Helmrath, J.J. Fong, C.M. Dekaney, S.J. Henning, Rapid expansion of intestinal secretory lineages following a massive small bowel resection in mice, Am. J. Physiol. Gastrointest. Liver Physiol. 292 (2007) G215–G222.
[52] F. Gaggini, B. Laleu, M. Orchard, L. Fioraso-Cartier, L. Cagnon, S. Houngninou-Molango, A. Gradia, G. Duboux, C. Merlot, F. Heitz, C. Szyndralewiez, P. Page, Design, synthesis and biological activity of original pyrazolo-pyrido-diazepine, -pyrazine and -oxazine dione derivatives as novel dual Nox4/Nox1 inhibitors, Bioorg. Med. Chem. 19 (2011) 6989–6999.
[53] A.P. Gilmore, T.W. Owens, F.M. Foster, J. Lindsay, How adhesion signals reach a mitochondrial conclusion–ECM regulation of apoptosis, Curr. Opin. Cell Biol. 21 (2009) 654–661.
[54] R.M. Jones, L. Luo, C.S. Ardita, A.N. Richardson, Y.M. Kwon, J.W. Mercante, A. Alam, C.L. Gates, H. Wu, P.A. Swanson, J.D. Lambeth, P.W. Denning, A.S. Neish, Symbiotic lactobacilli stimulate gut epithelial proliferation via Nox-mediated generation of reactive oxygen species, EMBO J. 32 (2013) 3017–3028.
[55] T. Goretsky, R. Dirisina, P. Sinh, N. Mittal, E. Managlia, D.B. Williams, D. Posca, H. Ryu, R.B. Katzman, T.A. Barrett, p53 mediates TNF-induced epithelial cell apoptosis in IBD, Am. J. Pathol. 181 (2012) 1306–1315.
[56] J. Grootjans, C.M. Hodin, J.J. de Haan, J.P. Derikx, K.M. Rouschop, F.K. Verheyen, R.M. van Dam, C.H. Dejong, W.A. Buurman, K. Lenaerts, Level of activation of the unfolded protein response correlates with Paneth cell apoptosis in human small intestine exposed to ischemia/reperfusion, Gastroenterology 140 (529–539) (2011) e523.
[57] N. Coant, S. Ben Mkaddem, E. Pedruzzi, C. Guichard, X. Treton, R. Ducroc, J.N. Freund, D. Cazals-Hatem, Y. Bouhnik, P.L. Woerther, D. Skurnik, A. Grodet, M. Fay, D. Biard, T. Lesuffleur, C. Deffert, R. Moreau, A. Groyer, K.H. Krause, F. Daniel, E. Ogier-Denis, NADPH oxidase 1 modulates WNT and NOTCH1 signaling to control the fate of proliferative progenitor cells in the colon, Mol. Cell. Biol. 30 (2010) 2636–2650.
[58] K.S. Bergstrom, V. Kissoon-Singh, D.L. Gibson, C. Ma, M. Montero, H.P. Sham, N. Ryz, T. Huang, A. Velcich, B.B. Finlay, K. Chadee, B.A. Vallance, Muc2 protects against lethal infectious colitis by disassociating pathogenic and commensal bacteria from the colonic mucosa, PLoS Pathog. 6 (2010) e1000902.
[59] M. Kim, H. Ashida, M. Ogawa, Y. Yoshikawa, H. Mimuro, C. Sasakawa, Bacterial interactions with the host epithelium, Cell Host Microbe 8 (2010) 20–35.
[60] R.S. Esworthy, B.W. Kim, Y. Wang, Q. Gao, J.H. Doroshow, T.L. Leto, F.F. Chu, The Gdac1 locus modifies spontaneous and Salmonella-induced colitis in mice deficient in either Gpx2 or Gpx1 gene, Free Radic. Biol. Med. 65 (2013) 1273–1283.
[61] S.S. Dhillon, R. Fattouh, A. Elkadri, W. Xu, R. Murchie, T. Walters, C. Guo, D. Mack, H.Q. Huynh, S. Baksh, M.S. Silverberg, A.M. Griffiths, S.B. Snapper, J.H. Brumell, A.M. Muise, Variants in nicotinamide adenine dinucleotide phosphate oxidase complex components determine susceptibility to very early onset inflammatory bowel disease, Gastroenterology 147 (680–689) (2014) e682.
[62] P. Hayes, S. Dhillon, K. O'Neill, C. Thoeni, K.Y. Hui, A. Elkadri, C.H. Guo, L. Kovacic, G. Aviello, L.A. Alvarez, A.M. Griffiths, S.B. Snapper, S.R. Brant, J.H. Doroshow, M.S. Silverberg, I. Peter, D.P. McGovern, J. Cho, J.H. Brumell, H.H. Uhlig, B. Bourke, A.A. Muise, U.G. Knaus, Defects in NADPH oxidase genes NOX1 and DUOX2 in very early onset inflammatory bowel disease, Cell. Mol. Gastroenterol. Hepatol. 1 (2015) 14.
[63] G.R. Drummond, S. Selemidis, K.K. Griendling, C.G. Sobey, Combating oxidative stress in vascular disease: NADPH oxidases as therapeutic targets, Nat. Rev. Drug Discov. 10 (2011) 453–471.
[64] B. Rada, T.L. Leto, Oxidative innate immune defenses by Nox/Duox family NADPH oxidases, Contrib. Microbiol. 15 (2008) 164–187.
[65] H.H. Uhlig, Monogenic diseases associated with intestinal inflammation: implications for the understanding of inflammatory bowel disease, Gut 62 (2013) 1795–1805.
[66] M. Hausmann, K. Leucht, C. Ploner, S. Kiessling, A. Villunger, H. Becker, C. Hofmann, W. Falk, M. Krebs, S. Kellermeier, M. Fried, J. Scholmerich, F. Obermeier, G. Rogler, BCL-2 modifying factor (BMF) is a central regulator of anoikis in human intestinal epithelial cells, J. Biol. Chem. 286 (2011) 26533–26540.